

# Multistability and transient dynamics on networked systems

by

Kalel Luiz Rossi

M.S. Physics, Federal University of Parana  
B.S. Physics, Federal University of Parana

Submitted to the Department of Physics  
in partial fulfillment of the requirements for the degree of

## DOCTOR OF PHYSICS

at the

# MASSACHUSETTS INSTITUTE OF TECHNOLOGY

December 2024

© 2024 Kalel Luiz Rossi. All rights reserved.

The author hereby grants to MIT a nonexclusive, worldwide, irrevocable, royalty-free license to exercise any and all rights under copyright, including to reproduce, preserve, distribute and publicly display copies of the thesis, or release the thesis under an open-access license.

Authored by: Kalel Luiz Rossi  
Institute for Chemistry and Biology of the Marine Environment  
December 1, 2024

Certified by: Ulrike Feudel  
Professor, Thesis Supervisor

Accepted by: Primus Castor  
Professor of Wetlands Engineering



# **Multistability and transient dynamics on networked systems**

by

Kalel Luiz Rossi

Submitted to the Department of Physics

on December 1, 2024 in partial fulfillment of the requirements for the degree of

DOCTOR OF PHYSICS

## **ABSTRACT**

Thesis supervisor: Ulrike Feudel

Title: Professor



# Acknowledgments

Write your acknowledgments here.



# Contents

<i>List of Figures</i>	9
<i>List of Tables</i>	13
<b>1 Introduction</b>	<b>15</b>
1.1 networks . . . . .	15
1.2 multistability . . . . .	16
1.3 metastability . . . . .	16
<b>2 Methodology</b>	<b>17</b>
2.1 multistability . . . . .	17
<b>3 Small changes at single nodes can shift global network dynamics</b>	<b>19</b>
3.1 Introduction . . . . .	19
3.2 Methodology . . . . .	21
3.3 Results . . . . .	24
3.3.1 Introduction to dynamical malleability . . . . .	24
3.3.2 Comprehensive view of dynamical malleability . . . . .	26
3.3.3 Unpredictability of dynamical malleability . . . . .	29
3.3.4 Ratio of short to long-range connections . . . . .	31
3.3.5 Multistability . . . . .	32
3.3.6 Distributions of samples . . . . .	34
3.4 Discussions and conclusions . . . . .	35
3.4.1 Summary . . . . .	35
3.4.2 Mechanisms for dynamical malleability . . . . .	36
3.4.3 Mechanisms for the fluctuations . . . . .	36
3.4.4 Relation to statistical physics and scaling . . . . .	38
3.4.5 Generality of the behavior . . . . .	38
3.4.6 Practical importance of malleability . . . . .	39
3.4.7 Future research and conclusions . . . . .	39
<b>4 Dynamical properties and mechanisms of metastability: a perspective in neuroscience</b>	<b>41</b>
4.1 Introduction . . . . .	42
4.2 Short summary of metastability in the brain . . . . .	43
4.2.1 Observations of metastability . . . . .	43
4.2.2 Current formulations of metastability . . . . .	45

4.2.3	The common thread . . . . .	46
4.3	Metastability in state space . . . . .	47
4.3.1	Stability and invariance - initial concepts . . . . .	47
4.3.2	Metastability and almost-invariance - definition . . . . .	48
4.3.3	Dynamics-based mechanisms for metastability . . . . .	50
4.3.4	Subtypes of metastability . . . . .	55
4.4	Conclusions and outlook . . . . .	56
4.4.1	Models . . . . .	58
4.4.2	Brief notion of almost-invariant sets . . . . .	60
<b>A</b>	<b>Code listing</b>	<b>61</b>

# List of Figures

- 3.1 Sketch to illustrate the dynamical malleability in a typical transition to phase synchronization. Each realization of the system's parameters leads to a different transition to synchronization, i.e. a different curve in the figure. Realizations may differ from the others, for instance, in the parameter of a single unit. We see that the transitions to synchronization are different, as both the critical value of the coupling strength and the profile of the transitions differ, with the magnitude of malleability peaking during the transitions. Fixing the coupling strength, we can also look at the distribution of the degree of phase synchronization across samples (purple inset). . . . . 22
- 3.2 Transition to phase synchronization and the effect of a single-unit change. The figure shows the color-coded phases  $\theta$  of all oscillators in the network and the degree of phase synchronization  $r(t)$  (green line) across time for Watts-Strogatz networks. The coupling strength  $\epsilon$  is fixed at  $\epsilon = 4.51282$  and the natural frequencies  $\omega_i$  in the first row are the same, generated by randomly drawing from a Gaussian distribution with zero mean and unitary standard deviation. Networks in the left column are two-nearest-neighbor lattices (rewiring probability  $p = 0$ ); the short-range connections in these networks are then rewired in the following columns, with probability  $p = 0.08733$  in the second column,  $p = 0.19684$  in the third, and  $p = 1.0$  in the fourth (leading to random networks). Increasing the proportion of long-range connections thus leads generally to more phase-synchronized networks. In the second and third rows, the natural frequency  $\omega_i$  of a single unit  $i$  (indicated by the gray arrows) is changed to a new value  $\omega_i \rightarrow \omega_{\text{new}} = 3.0$ , with all other parameters being kept fixed. The units shown in the figure were those which led to the smallest (second row) or highest (third row) degree of phase synchronization  $R$  out of all  $N = 501$  units in the network for each value of  $p$ . Initial conditions were the same for all simulations, and were randomly drawn between 0 and  $2\pi$ . . . . . 25

- 3.3 **Transitions to phase synchronization and dynamical malleability.** Networks under Watts-Strogatz (WS) and distance-dependent (DD) topologies reach phase synchronization through either an increase in coupling strength  $\epsilon$  (given the topology has a sufficient amount of long-range connections) or by switching short-range connections to long-range. Fluctuations in the degree of phase synchronization  $R$  between samples increase during the transitions, as can be seen by the differences in the same-colored curves and by  $\Delta := R_{\max} - R_{\min}$ . Starting from a natural frequency sequence originally drawn from a Gaussian distribution (thicker lines), the other samples (thinner lines) can be generated by shuffling the natural frequencies or by switching the natural frequency of one unit to  $\omega_{\text{new}} = 3$ . For intermediate networks (purple and green curves), the increase in the fluctuations (i.e. in dynamical malleability) extends for a wide range of parameters and becomes considerably large. Each panel contains  $501 = N$  realizations, with rewiring probabilities fixed for the coupling transition, with values shown in the legend, and coupling strength fixed in the topology transition at  $\epsilon = 4.51282$  for WS and  $\epsilon = 6.46154$  for DD. The initial conditions are the same across all realizations, and are randomly distributed from 0 to  $2\pi$ . The curves of  $\Delta$  are qualitatively similar with other dispersion measures, such as standard deviation, a possible difference being that the curves may be slightly shifted, as the measures can peak at slightly different values of the control parameter. We remark that the parameter values used in the simulations were generated as described in Section 3.2 and correspond to the typical behaviors in the system. . . . .
- 3.4 **Dynamical malleability increases around the regions of transition to phase synchronization.** The surface on the left shows the average degree of phase synchronization  $\bar{R}$  across the ensemble (1000 realizations of shuffled natural frequencies). The region of high phase synchronization is clearly seen for sufficiently high coupling strength  $\epsilon$  and rewiring probability  $p$ . The colored lines correspond to the parameter values shown in Fig. 3.3. The right panel displays  $\Delta$ , the difference between the most and least synchronized realizations for each pair  $(p, \epsilon)$ , and we see that the fluctuations from sample to sample increase during the transitions to phase synchronization. The green and purple curves remain close to the region of transition for all  $\epsilon \gtrless 1$ , such that their fluctuations do not decrease with an increase in  $\epsilon$ . The figure uses Gouraud interpolation to ease visualization by smoothing the curves with a linear interpolation. . . . .

- 3.5 **Fluctuations in dynamically malleable systems are unpredictable.** Panel (a) shows the average phase synchronization  $R$  for fixed coupling strength  $\epsilon = 4.51282$  and rewiring probability  $p = 0.08733$  for different 20 shuffles of the natural frequencies  $\{\omega_i\}$  and samples of networks generated by the Watts-Strogatz algorithm. For ease of visualization, the networks are ordered such that the highest network ids correspond to higher synchronization for Shuffle id = 1. For each shuffle, the network with the highest  $R$  is marked with a red rectangle. We thus see that no network synchronizes more for all shuffles:  $R$  is a function of both the specific frequency and topology samples. Panel (b) shows the changes  $\delta R$  in the phase synchronization  $R$  when the natural frequency of each unit is changed by an amount  $\delta\omega$ , such that  $\omega_i \rightarrow \omega_i + \delta\omega$ . Other parameters are fixed, in particular  $p = 0.1145$  and  $\epsilon = 4.51282$ . There is a rough threshold (indicated by the black dashed lines), below which changing  $\omega_i$  does not significantly alter  $R$  ( $\delta R < 0.1$  for the figure). Furthermore, changing the frequency does not have a monotonic impact on the change in  $R$ : small alterations in  $\omega_i$ , above the threshold, can have the same impact on  $R$  as bigger alterations. . . . .

30

3.6 **Dynamical malleability peaks within a narrow interval in the relation of short-range to long-range connections.** Panel (a) illustrates the short-range (blue) and long-range (red) connections from the yellow unit for  $d = 2$ . Panel (b) shows the sample-to-sample fluctuations in the phase synchronization measured as the standard deviation  $\chi$  of the distribution function of  $R$  against the ratio  $\kappa$  of short-range to long-range connections calculated for several distinct topologies  $p$  and  $\alpha$ . The green curve corresponds to the distance-dependent networks, with  $\epsilon = 6.46154$  and 501 realizations per  $\alpha$ ; purple corresponds to Watts-Strogatz networks,  $\epsilon = 4.51282$  and 1501 realizations per  $p$ . The bottom axis show the values of  $p$  and  $\alpha$  for the respective ticks in  $\kappa$  (note that values of  $\alpha$  are not equally spaced). . . . .

32

3.7 **Multistability in WS networks.** Phase synchronization and its dispersion for 501 different shuffles (thinner lines) of the initial conditions, taken from the original initial conditions (thicker lines) used throughout the rest of this work. All other parameters are fixed, including the natural frequencies as the original frequency distribution. The coupling strength  $\epsilon$  (left panel) and rewiring probabilities  $p$  (right panel) are the same ones used for WS networks in Fig. 3.3. The multistable behavior is thus very similar to what we observed before by changing the frequencies (Fig. 3.3(a) and (e)), and so shuffling the initial conditions for this network also leads to large fluctuations in the phase synchronization. . . . .

33

3.8	<b>Distributions of <math>R</math> due to shuffling frequencies or initial conditions.</b> Each panel contains the distribution of the mean degree of phase synchronization $R$ across 20000 shuffles of natural frequencies (in purple) or initial conditions (orange) for Watts-Strogatz networks. The rewiring probabilities $p$ are indicated on the right of each row, and are the same as used in Fig. 3.3(a); the coupling strengths $\epsilon$ are indicated on the top of each column. Bin size is 0.005, and the probability for each bin is calculated as the occupation of the bin divided by the total occupation across all bins, and is shown in logarithmic scale. . . . .	35
4.1	<b>Brain activity typically evolves as a sequence of well-defined regimes that are transient but long lived.</b> The panels illustrate observations taken from the literature, namely EEG microstates [144] (A), firing rate states identified via hidden-Markov-modelling (HMM) [28] (B), UP and DOWN states [104] (C), cortical wave patterns [206] (D), seizure-like activity [217] (E), and bursting in central pattern generators [184] (F). Each observation is explained in detail in the main text, and is classified into subtypes of metastability that we define in the Sec. 4.3.4. . . . .	44
4.2	<b>Formulations of metastability in the neuroscience literature.</b> A common theme among these is the presence of transitions between certain aspects of the system's dynamics (e.g., between activity patterns). The upper part of the figure (A-F) illustrates what these aspects are in each formulation, and the bottom part (G-H') shows characteristics of the transitions. Further details are available in the main text. . . . .	46
4.3	<b>Illustration of multistability versus metastability.</b> Panels A and A' illustrate the behavior of a ball on a double-well landscape, representing a multistable system. The stable and unstable equilibria are represented by green and red circles, respectively. In A, the ball is shown on the landscape to converge to the equilibrium on the right, where it stays indefinitely (equilibria are invariant). In A', a possible corresponding trajectory is shown in state space. The green curves leaving the unstable equilibrium denote its stable manifold, while the red curves denote the unstable manifold. In B, we suppose there is a demon kicking the ball and thus introducing white noise to its dynamics. This now makes the ball switch eternally between the two wells, and effectively transforms the previous equilibria (not invariant anymore, represented as faded circles) into metastable regions (which are almost-invariant), represented illustratively in B' by the purple and green ellipses. . . . .	49
4.4	<b>Dynamics-based mechanisms of metastability.</b> Each column corresponds to a distinct mechanism. The first row (A-E) shows a representative time-series, with alternations between metastable regimes, each receiving a distinct color. The second row (A'-E') shows the state space of each system with the trajectory corresponding to the time-series above. The third row (A''-E'') shows the distribution of residence times in each metastable region for several trajectories. Further details are discussed in the main text and Supplemental Material. . . . .	52

## List of Tables



# Chapter 1

## Introduction

### 1.1 Networks

Several natural and artificial systems are composed of separate entities that interact together, forming networks - or, at least, they can be approximately modelled as networks. Often, these interactions generate complex behaviors, which would not exist without the interactions. For instance, neural circuits blabla.

A major area of research today is to understand precisely how this large-scale complex dynamics emerges from the interactions between units in networks. This ranges from setting up experiments XX, modelling to a high precision, and also building the basic theory that aims to describe the fundamental aspects of these networks. For this thesis we have focused on the latter case, aiming to study the fundamental behavior of simple, non-specific, networks. To do this, we have relied on a second layer of abstraction: often, networks can be modelled as dynamical systems following ODEs of the general form:

$$\dot{x}_i = f(x_i) + g(x) \quad (1.1)$$

where XX. Introduce topology, connections. Examples? power grids and neural networks and kuramoto?

This abstraction is quite helpful, because systems of this form can be studied using techniques from dynamical systems theory. XX?

Among the plethora of important dynamics arising in networks, we have in this thesis focused on three particular behaviors: malleability, multistability and metastability. Although separate, they are intrinsically related, as we will see. For the first two, we have focused on how they are controlled by the network's topology.

The first behavior we have studied is *dynamical malleability*, which refers to the capacity of a network to change its dynamics when the individual parameters of units or connections are changed. We studied this behavior in Kuramoto oscillator networks of the form

$$\dot{\theta} \dots \quad (1.2)$$

These networks serve as paradigmatic models to understand emergent behavior - in particular, synchronization - in complex networks. They can be derived as an approximation for

generic coupled limit cycle oscillators under weak coupling []. Although it does not model a particular real-world system, it has been used as a simple model for large-scale brain networks [] and power grids [] ?. Originally used to describe chemical oscillations XX.

## 1.2 Multistability

## 1.3 Metastability

usefulness for computations?

# Chapter 2

## Methodology

### 2.1 Multistability



# Chapter 3

## Small changes at single nodes can shift global network dynamics

Kalel L. Rossi<sup>1</sup>, Roberto C. Budzinski<sup>2,3,4</sup>, Bruno R. R. Boaretto<sup>5</sup>, Lyle E. Muller<sup>2,3,4</sup>, Ulrike Feudel<sup>1</sup>

<sup>1</sup> Theoretical Physics/Complex Systems, ICBM, Carl von Ossietzky University of Oldenburg, Oldenburg, Lower Saxony, Germany

<sup>2</sup> Department of Mathematics, Western University, London, Ontario, Canada,

<sup>3</sup> Brain and Mind Institute, Western University, London, Ontario, Canada,

<sup>4</sup> Western Academy for Advanced Research, Western University, London, Ontario, Canada,

<sup>5</sup> Institute of Science and Technology, Federal University of São Paulo, São José dos Campos, São Paulo, Brazil

**Abstract.** Understanding the sensitivity of a system's behavior with respect to parameter changes is essential for many applications. This sensitivity may be desired - for instance, in the brain, where a large repertoire of different dynamics, particularly different synchronization patterns, is crucial - or may be undesired - for instance, in power grids, where disruptions to synchronization may lead to blackouts. In this work, we show that networks of coupled phase oscillators with nonlinear interactions can acquire a very large and complicated sensitivity to changes made in either their units' parameters or in their connections. Even modifications made to a parameter of a single unit can radically alter the global dynamics of the network in an unpredictable manner. This occurs over a wide parameter region, around the network's transitions to phase synchronization. We argue that this is a widespread phenomenon that can be expected in real-world systems, extending even beyond networks of oscillators.

### 3.1 Introduction

Several systems of practical and theoretical importance are composed of, or can be modeled as, networks of interacting units. Examples from different research areas include power grids

(networks of producers and consumers of electrical energy) [145], food webs [57], networks of electronic elements [46], coupled lasers [153], and neurons in the brain [209]. An important question is how the dynamics of single units impact the network's overall dynamics, and what happens if these units are modified. What happens to the dynamics if the units' parameters change? For instance, in ecological systems, what happens if the reproduction rate of a prey increases? In power grids, can a change in the parameters of a single generator cause a large disruption, such as a blackout? Also, what happens if the units' dynamical states are modified, e.g. by shocking the units into a different state? In the brain, how can an epileptic seizure be stopped by employing a current pulse in one particular brain region? These questions highlight the idea that a regime in which single-unit-changes can alter the whole network's behavior can be either dangerous or advantageous, and is an important topic of research which we address in this work.

In both power grids and the brain, an important phenomenon is synchronization, i.e. the coherence of frequencies or even phases of oscillations. For example, it is crucial for power grids to have their elements synchronized in the 50 – 60 Hz regime [220]. Moreover, several functional roles have been ascribed to synchronization in the brain [68, 209, 187]. For systems in which synchronization is an essential process for functioning, the question of sensitivity with respect to perturbations becomes particularly important. This has been recognized in the literature, and various types of perturbations have been considered to study the vulnerability either of the synchronized state itself or of the transition to synchronization [159, 11].

In this work, we show that systems become very sensitive to changes in parameters during transitions to synchronization, such that even changes to parameters of single units can radically alter the dynamics of the whole system. We call this phenomenon *dynamical malleability* [31], characterized by the fluctuations in network behavior caused by changes in the units' parameters or connections. Dynamical malleability can cause problems in real-world systems in two major ways: (i) the fluctuations in the dynamics can have a large magnitude, which can lead to drastic changes in the system's spatiotemporal dynamics and (ii) fluctuations are complicated and hard to predict, so that it is unclear which units or new parameter values can keep the networks in a similar synchronization state, and which others can not. Indeed, no method available in the literature to describe phase synchronization worked satisfactorily to predict the fluctuations we observe. This clearly important issue for the design and control of systems motivates our study to analyze the mechanisms that lead to these large fluctuations.

To address it concretely, we study networks of Kuramoto oscillators organized in ring lattices. They constitute a paradigmatic model for synchronization [120, 2, 175] and have been established as a model for real-world systems like the brain [163, 37, 175], Josephson junctions [106, 46], and chemical oscillators [134, 151]. The Kuramoto oscillators are phase oscillators coupled through a sine function of their phase differences. Networks with these units are well-known to have a transition from desynchronization (incoherent phases) to frequency synchronization (i.e. phase-locking, meaning constant phase differences [159]) and to phase synchronization (small phase differences) [177] as the coupling strength between units increases [175, 2].

In this work, we connect the oscillators in either of two classes of network topologies, which are of theoretical and practical importance [5]: Watts-Strogatz [216, 98, 199] and

distance-dependent [176, 181]. They have very distinct properties, but in both a change in the topology from short-range to long-range connections leads to a transition to phase synchronization in the networks [90, 176]. During the transitions to phase synchronization, when the systems are only partially phase synchronized, they become dynamically malleable (i.e., sensitive to parameter changes), as illustrated in Fig. 3.1.

Furthermore, we also show that the number of attractors of the Watts-Strogatz networks increases during their transitions to phase synchronization, meaning that these systems also become especially sensitive to perturbations made to their units' states. This goes in line with recent studies for Kuramoto oscillators with identical frequencies [198, 222, 205] and for Kuramoto oscillators with inertia [75]. This increased multistability acts as a dynamical mechanism that can further increase the dynamical malleability.

Therefore, despite the wide literature and importance of synchronization, this phenomenon we describe of increased sensitivity to parameter changes, with complicated, hard-to-predict consequences to the synchronization, and which can be accompanied by multistability, has so been under-explored in the literature. Although reported sporadically in some recent works [158, 197, 12, 30], it has not been the focus, and thus has not been fully explored, until now. This becomes especially relevant when we note that the behavior is widespread, extending well beyond the Kuramoto networks studied here, as supported by our observations in a variety of topologies, by similar observations in spiking [31] and bursting [30] neural networks, in cellular automata (which we exemplify in the Supplemental Material), and, importantly, by the statistical physics theory of finite-size effects on phase transitions, which we discuss later in the paper.

We therefore hope to demonstrate the importance of dynamical malleability, and to encourage further theoretical advancements in this area, which are needed to properly describe the wide range of behaviors and to offer tools for practical applications.

## 3.2 Methodology

In the Kuramoto model [120, 121], each oscillator is described by a phase which evolves in time according to

$$\dot{\theta}_i = \omega_i + \epsilon \sum_{j=1}^N A_{ij} \sin(\theta_j - \theta_i), \quad (3.1)$$

where  $\theta_i(t)$  is the phase of the  $i$ -th oscillator at time  $t$ ,  $\omega_i$  is its natural frequency,  $\epsilon$  is the coupling strength,  $N$  is the number of oscillators, and  $A_{ij}$  is the  $(i, j)$ -th element of the adjacency matrix  $\mathbf{A}$ . Throughout this work, we initially draw each frequency randomly from a Gaussian distribution with mean  $\mu = 0.0$  and standard deviation  $\sigma = 1.0$ , generating a sequence  $\{\omega_i\}, i = 1, \dots, N$ . Then, different realizations can (i) shuffle these frequencies, generating another sequence  $\{\omega_i\}_{\text{shuffled}} = \text{shuffle}(\{\omega_i\})$ ; or (ii) switch the frequency of one selected unit to another value  $\omega_{\text{new}}$ .

The networks in this work are coupled in a ring lattice of  $N = 501$  units with periodic boundary conditions, and follow one of two classes of topology. The first class is the Watts-Strogatz (WS) [216], which interpolates between regular and random topologies with

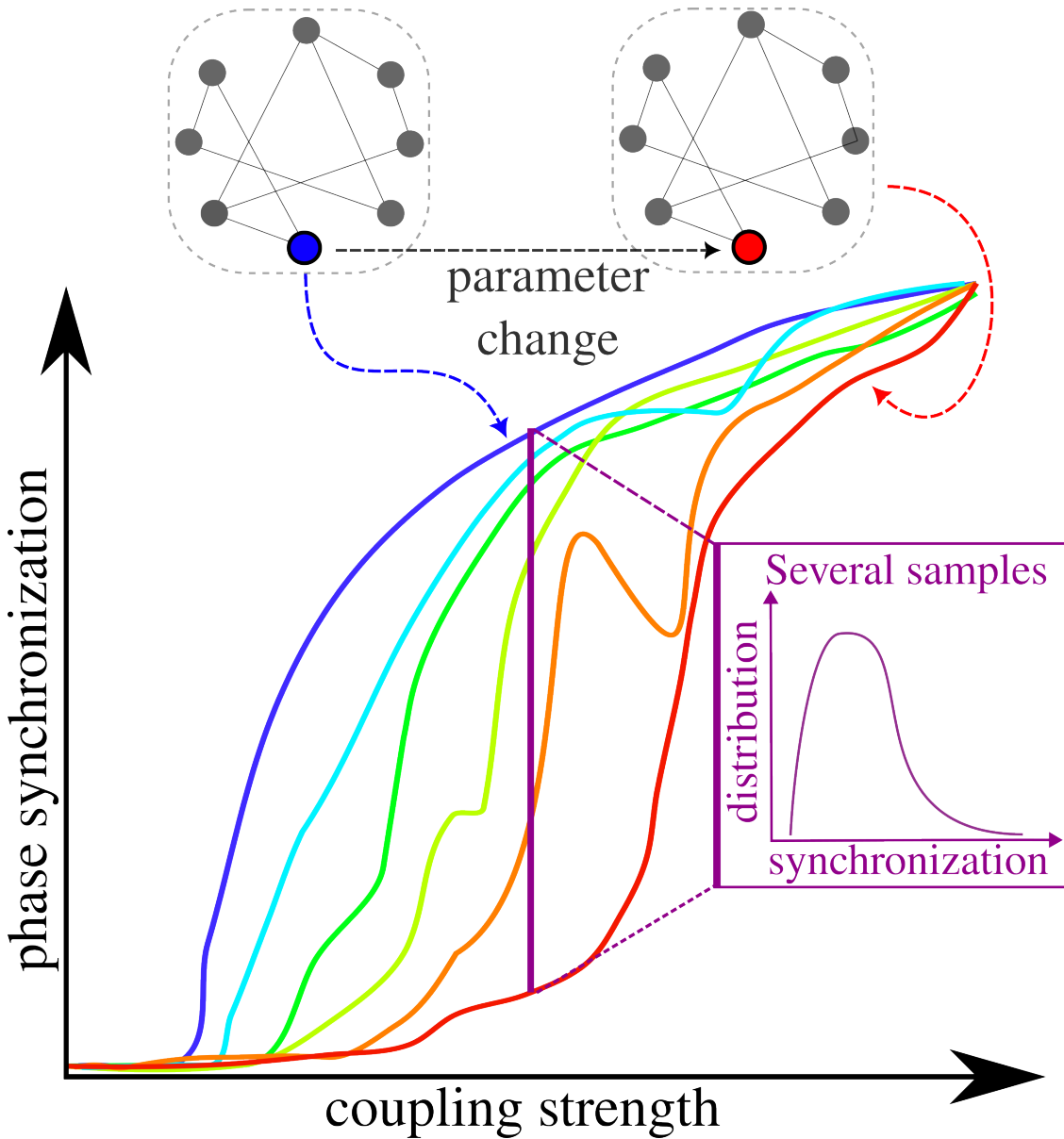


Figure 3.1: Sketch to illustrate the dynamical malleability in a typical transition to phase synchronization. Each realization of the system's parameters leads to a different transition to synchronization, i.e. a different curve in the figure. Realizations may differ from the others, for instance, in the parameter of a single unit. We see that the transitions to synchronization are different, as both the critical value of the coupling strength and the profile of the transitions differ, with the magnitude of malleability peaking during the transitions. Fixing the coupling strength, we can also look at the distribution of the degree of phase synchronization across samples (purple inset).

a parameter  $p$ , the rewiring probability: at one extreme ( $p = 0$ ), the topology is a  $k$ -nearest-neighbor lattice. From it, connections are randomly chosen according to the probability  $p$  and rewired to another randomly chosen connection. In doing this, the networks have a

significant decrease in the mean distance between nodes, but remain very clustered, generating small-world topologies. The other extreme ( $p = 1$ ) is then a random topology. These networks are unweighted, so their adjacency matrix's elements are  $A_{ij} = 1$  if  $i$  and  $j$  are connected, and 0 otherwise.

The second class of networks follows a distance-dependent (DD) powerlaw scheme, in which any given node receives connections with weights decaying based on the distance to it. Each element of the adjacency matrix is  $A_{ij} = \frac{1}{\eta(\alpha)(d_{ij})^\alpha}$ , where  $d_{ij}$  is the edge distance between oscillators  $i$  and  $j$ , defined as  $d_{ij} = \min(|i-j|, N-|i-j|)$ , and  $\eta(\alpha)$  is a normalization term given by:  $\eta(\alpha) = \sum_{j=1}^{N'} \frac{2}{j^\alpha}$ , such that the temporal evolution of the phases can be written as:

$$\dot{\theta}_i = \omega_i + \frac{\epsilon}{\eta(\alpha)} \sum_{j=1}^{N'} \frac{1}{j^\alpha} [\sin(\theta_{i+j} - \theta_i) + \sin(\theta_{i-j} - \theta_i)], \quad (3.2)$$

where  $N' = \frac{N-1}{2}$  denotes half the amount of units to which  $i$  is connected to (one half of the ring's length, discounting the unit  $i$  itself). The equation explores the symmetry in the network to switch the summation across the network to a summation across only half, multiplied by 2. The powerlaw decay is thus controlled by  $\alpha$ , the locality parameter. For  $\alpha = 0$ , the network is globally coupled with equal weights between every node. As  $\alpha$  increases, the weights are redistributed, so that closer units (in terms of edge-distance) have bigger weights. At the extreme of  $\alpha \rightarrow \infty$ , only first-neighbors are connected.

The two classes have similarities: they have topologies dominated by short-range connections at one extreme and by long-range connections at another [188, 94]. They also have differences: the first class is sparsely connected, the other densely; the first has link-disorder (different rewirings lead to different networks), the second does not.

Integration was performed using the Tsitouras 5/4 Runge-Kutta (Tsit5) method for Watts-Strogatz networks, and an adaptive order adaptive time Adams Moulton (VCABM) method for distance-dependent networks. The integrator method was chosen for distance-dependent networks for increased simulation speed, and results were robust to different integration schemes. All methods used the DifferentialEquations.jl package [171], written in the Julia language [21]. Additional computational packages used were PyPlot [99] for plotting and DrWatson.jl [50] for code management. The code used for simulations is accessible in the repository [179], with the parameters used in the simulations. In particular, the control parameters we used ( $\alpha$ ,  $p$  and  $\epsilon$ ) were generated from a uniform distribution in the range of parameters showing interesting behaviors (e.g. the transitions to synchronization), then rounded to five decimal places and used in the simulations (in the case of  $p$ , the distribution was uniform in the log scale). These values are reported in all figures and text, and we emphasize that no value was chosen specifically by hand: the behaviors we show in the figures are typical of the systems and can be obtained by randomly generating other values for the parameters.

We quantify the degree of phase synchronization of the network through the standard Kuramuro order parameter [120, 121, 2], which is the circular average of the units' phases

$$r(t) = \frac{1}{N} \left| \sum_{j=1}^N \exp(i\theta_j(t)) \right|, \quad (3.3)$$

with  $i = \sqrt{-1}$ . The quantifier ranges from 0 to 1: if  $r(t) = 1$ , all the phases are the same, and the system is completely globally phase-synchronized; if  $r(t) = 0$ , each oscillator has a pair that is completely out-of-phase, and the system can be completely globally phase-desynchronized or in a twisted state with units having distinct but linearly spaced phases. We typically describe networks by the temporal average  $R := \frac{1}{T} \sum_t r(t)$  of their phase synchronization, with  $T$  being the total simulation time excluding transients.

## 3.3 Results

### 3.3.1 Introduction to dynamical malleability

The networks we study here, described in Eq. (3.1), follow the basic phenomenology of transitions to synchronization in Kuramoto networks [120, 2]. For very small coupling strengths  $\epsilon$ , the oscillators are effectively uncoupled, and the phases oscillate without any significant correlation. As this  $\epsilon$  increases, the instantaneous frequencies  $\dot{\theta}_i$  align first, and the units' phases become locked, but not aligned: the system becomes frequency but not phase synchronized [159].

Then, whether the phases can align or not depends on the topology [142, 90]. In a two-nearest neighbor lattice, where only four nearby units are connected (two on each side), there is a topological limitation in the spread of interactions across the network that makes the oscillators arrange themselves in shorter-range patterns (Fig. 3.2(a)) (an exception might occur if the coupling strength is extremely high, much bigger than the relevant values studied here). If the short-range connections are randomly rewired to long-range connections, following for instance the Watts-Strogatz (WS) algorithm, the shorter-range patterns give way to longer-range patterns, and the oscillators start to phase synchronize ((b) and (c)), until eventually a strong (though not complete) phase synchronization (PS) is reached (d). This occurs at different stages for each realization: for instance, panels (c) and (k) reach a high degree of PS, with the longer-range patterns, but panel (g) does not.

In Fig. 3.2, the natural frequencies  $\{\omega_i\}(i = 1, \dots, N)$  were kept constant across panels (a)-(d). Changing the frequencies, keeping the initial conditions  $\{\theta_i(0)\}(i = 1, \dots, N)$  fixed, leads to a different realization (also called sample), with possibly different dynamics. If the frequency of a single unit  $\omega_i$  is changed to an arbitrary new value, for instance  $\omega_{\text{new}} = 3$ , the network's behavior can be significantly altered (panels (e)-(h)). This is especially the case for networks with intermediate rewiring probabilities  $p$ , in which this single unit frequency change can bring the network from high to very low phase synchronization (panels (c) to (g)). The instantaneous frequencies typically remain synchronized, though their values might change. For random networks, phase synchronization is always maintained, though the instantaneous frequency values may also change.

Figure 3.2 thus illustrates that the long-term dynamics and phase synchronization differ in each realization. The realizations, created by changing the natural frequency of one unit, are distinct dynamical systems, so it is not surprising to observe distinct long-term dynamics. It is, however, interesting to observe how large these changes in dynamics can be, and how they depend on the topology. For instance, in networks of intermediate  $p$  (second and third columns of Fig. 3.2), the phase synchronization changes drastically. In

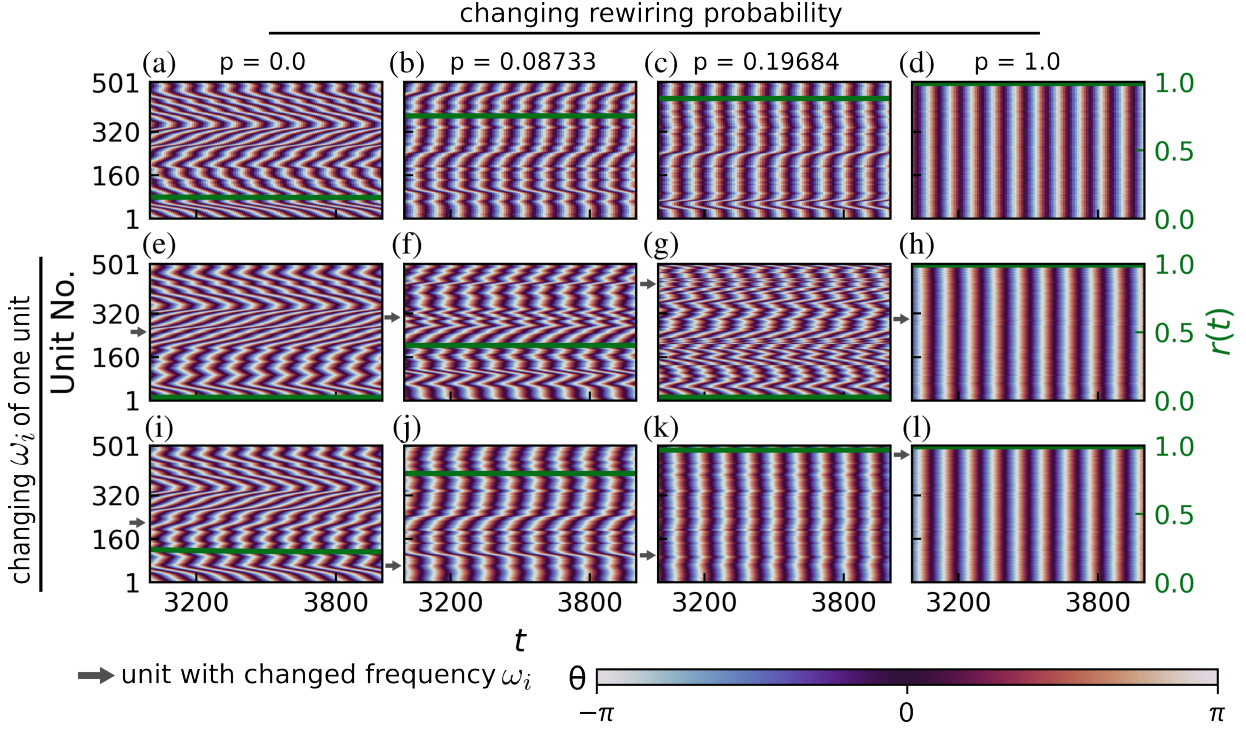


**Figure 3.2: Transition to phase synchronization and the effect of a single-unit change.** The figure shows the color-coded phases  $\theta$  of all oscillators in the network and the degree of phase synchronization  $r(t)$  (green line) across time for Watts-Strogatz networks. The coupling strength  $\epsilon$  is fixed at  $\epsilon = 4.51282$  and the natural frequencies  $\omega_i$  in the first row are the same, generated by randomly drawing from a Gaussian distribution with zero mean and unitary standard deviation. Networks in the left column are two-nearest-neighbor lattices (rewiring probability  $p = 0$ ); the short-range connections in these networks are then rewired in the following columns, with probability  $p = 0.08733$  in the second column,  $p = 0.19684$  in the third, and  $p = 1.0$  in the fourth (leading to random networks). Increasing the proportion of long-range connections thus leads generally to more phase-synchronized networks. In the second and third rows, the natural frequency  $\omega_i$  of a single unit  $i$  (indicated by the gray arrows) is changed to a new value  $\omega_i \rightarrow \omega_{\text{new}} = 3.0$ , with all other parameters being kept fixed. The units shown in the figure were those which led to the smallest (second row) or highest (third row) degree of phase synchronization  $R$  out of all  $N = 501$  units in the network for each value of  $p$ . Initial conditions were the same for all simulations, and were randomly drawn between 0 and  $2\pi$ .

random networks ( $p = 1$ , fourth column), they preserve the phase synchronization but alter the instantaneous frequencies of the oscillators (seen in the figure by the number of vertical lines). We also note that the behavior we describe is typical of the systems, and the values of  $p$  and  $\epsilon$  used here were generated as described in Section 3.2. Since the fluctuations in the phase patterns (reflected in the phase synchronization) are clearer and more pronounced than the instantaneous frequency patterns, we now focus on the phase synchronization of the networks.

### 3.3.2 Comprehensive view of dynamical malleability

To obtain a comprehensive picture we now study an ensemble of samples obtained by shuffling the frequencies ( $\{\omega_i\}_{\text{original}} \rightarrow \{\omega_i\}_{\text{shuffled}} = \text{shuffle}(\{\omega_i\}_{\text{original}})$ ) or by changing the frequency of only a single unit to a new value ( $\omega_{i,\text{original}} \rightarrow \omega_{\text{new}}$ ). We show in Fig. 3.3 the transitions to phase synchronization with increasing coupling strength or with switching from short-range to long-range connections. As expected from Fig. 3.2 we also find a large dynamical malleability (sometimes simply called malleability) during the transitions.

We study two classes of topology, Watts-Strogatz (WS, small-world) and distance-dependent (DD), described in Sec. 3.2. We consider ensembles as collections of networks with fixed coupling strength  $\epsilon$  and topology (fixed rewiring probability  $p$  or locality parameter  $\alpha$ ) but distinct realizations of the natural frequencies  $\{\omega_i\}$  [41]. Each ensemble in the figure contains 501 samples (realizations). We present the results using the mean degree of phase synchronization  $R$  for each realization, and the gap  $\Delta := R_{\max} - R_{\min}$  between the most and least phase synchronized realizations in each ensemble. The gap  $\Delta$  is chosen simply to illustrate the wide range of  $R$  values clearly, and we remark that very similar curves are observed by using the standard deviation over samples.

In Fig. 3.3, thicker lines represent an “original” sequence of frequencies  $\{\omega\}_{\text{original}}$ , from which other realizations (light lines) are created by shuffling all frequencies or changing the frequency of one unit to a new value  $\omega_{\text{new}} = 3.0$ . Each sample is a different dynamical system, and has a different transition to phase synchronization, which occurs at different values of  $\epsilon$ ,  $p$ , or  $\alpha$ , and with a different profile (some have a small region of desynchronization while others do not, for instance).

This means that changing samples can lead to large changes in the behavior of the system, as we see throughout Fig. 3.3. First, we study the transitions induced by increasing the coupling strength  $\epsilon$  for four representative types of networks (panels (a)-(d)), characterized by four specific values of rewiring probability  $p$  and locality parameter  $\alpha$ .

In the red curves, networks are dominated by long-range connections, with  $p = 1$  (random) and  $\alpha = 0$  (all-to-all) and have a complete transition to phase synchronization (reaching  $R \sim 1$ ), with the dynamical malleability (measured by  $\Delta$ ) increasing during the transition and returning to zero after. The all-to-all case is the finite-size version of the system originally studied by Kuramoto [121], and the critical  $\epsilon$  values, when the transition occurs in each sample, are close to the  $\epsilon_c = \frac{2}{g(0)\pi} = \frac{2\sqrt{2}}{\sqrt{\pi}} \approx 1.596$  predicted in the thermodynamic (infinite network size) limit. Its finite-size scaling properties and behavior have also been studied in [91, 158]. It is worth mentioning that this parallel between random networks and all-to-all networks, which have similar phenomenology, has been described in other works. Both have the same scaling exponents, belonging to the mean-field type [188, 94].

In the green curves ( $p = 0.19684$  and  $\alpha = 1.538463$ ) some connections have been rewired in the Watts-Strogatz networks, and weights redistributed for distance-dependent networks, from long-range to effectively short-range connections. On average, phase synchronization  $R$  decreases, though still remaining high. Some samples of WS networks also start to display regions of desynchronization: after the initial transition to high  $R$ , a further increase in  $\epsilon$  can desynchronize them (visible in panels (a) and (c), for  $\epsilon$  roughly in [6, 7]). Therefore, the huge changes in  $R$  ( $\Delta \sim 0.99$ ) due to changing samples can be attributed to two effects: the difference in their critical coupling strength (when the transition begins) [92], and also in

their different post-transition behaviors (such as the desynchronization gaps that occur at different intervals of  $\epsilon$ .)

In the purple curves ( $p = 0.08733$  and  $\alpha = 1.76923$ ), even more short-range connections become present. Phase synchronization  $R$  on average decreases, while the fluctuations  $\Delta$  remain high and occur more evenly spread across samples.

Finally, for cyan curves ( $p = 0$ , two-nearest-neighbor chains and  $\alpha = 3$ , close to nearest-neighbor chains), the connections are short-range. Their phase synchronization is much smaller, and they do not reach a high degree of phase synchronization for any value  $\epsilon$  we tested. These networks with short-range connections still have some degree of malleability, but not as high as the previous two cases.

Returning to frequency synchronization, we mention that for weak coupling strengths (roughly below  $\epsilon \approx 3$ ), most of the samples in any ensemble are not frequency synchronized (see Fig. S3). Above this value, frequency synchronization becomes more common, especially for networks with more long-range connections, such that for sufficiently high coupling all samples become frequency synchronized. This is not the case for networks with mostly short-range connections ( $p \lesssim 0.01$ ), in which some samples do not reach frequency synchronization even despite strong coupling. The presence of frequency synchronization in the short-range networks is consistent with the literature [193, 2] showing that frequency synchronization in first-nearest-neighbor chains is possible for sufficiently high  $\epsilon$  in strictly finite systems. There are therefore also sample-to-sample fluctuations in the frequency synchronization of Kuramoto networks. They occur similarly to the fluctuations in phase synchronization, but are somewhat harder to visualize and have a less interesting dependence on parameters, justifying our focus on phase synchronization in this paper.

We now move to the topology induced transitions, which occur by switching from short-range to long-range connections (varying  $p$  and  $\alpha$ ) while keeping the coupling strength  $\epsilon$  fixed (Figs. (e-h)). A similar scenario occurs with a transition to phase synchronization, induced by changing either  $p$  or  $\alpha$ . The dynamical malleability increases during the transitions, reaching significant values for both shuffled realizations and single-unit changes. The nearest-neighbor networks show some malleability, while the long-range dominated ones (random or all-to-all) show no malleability. We note here that the transition for WS occurs at  $p \sim 0.1$ , so we plot the figures on logarithmic scale to show the full transition to synchronization. This transition was already reported for WS networks in [90], but the authors used a linear scale for  $p$  and missed the full details of the transition that we see here, especially the sample-to-sample fluctuations; for distance-dependent powerlaw networks, a transition in phase and frequency was reported in [176]. However, none of these references studied the sample-to-sample fluctuations.

We conclude that either shuffling or changing a single unit can significantly alter the behavior of these systems, leading to a large dynamical malleability, in some cases over a very large range of parameters. This is particularly strong for WS networks, reaching  $\Delta \sim 0.99$ , close to the maximum possible value of  $\Delta = 1.0$ . The distance-dependent networks have weaker fluctuations, though still significant, reaching up to  $\Delta \sim 0.7$ .

Furthermore, we note that the networks with intermediate  $p$  or  $\alpha$  and the short-range networks have dynamical malleability even for high  $\epsilon$ . This is consistent with the known increase in the fluctuations near a phase transition [91, 25, 88] because the networks with these parameters remain close to the topology-induced transition. This is illustrated for WS

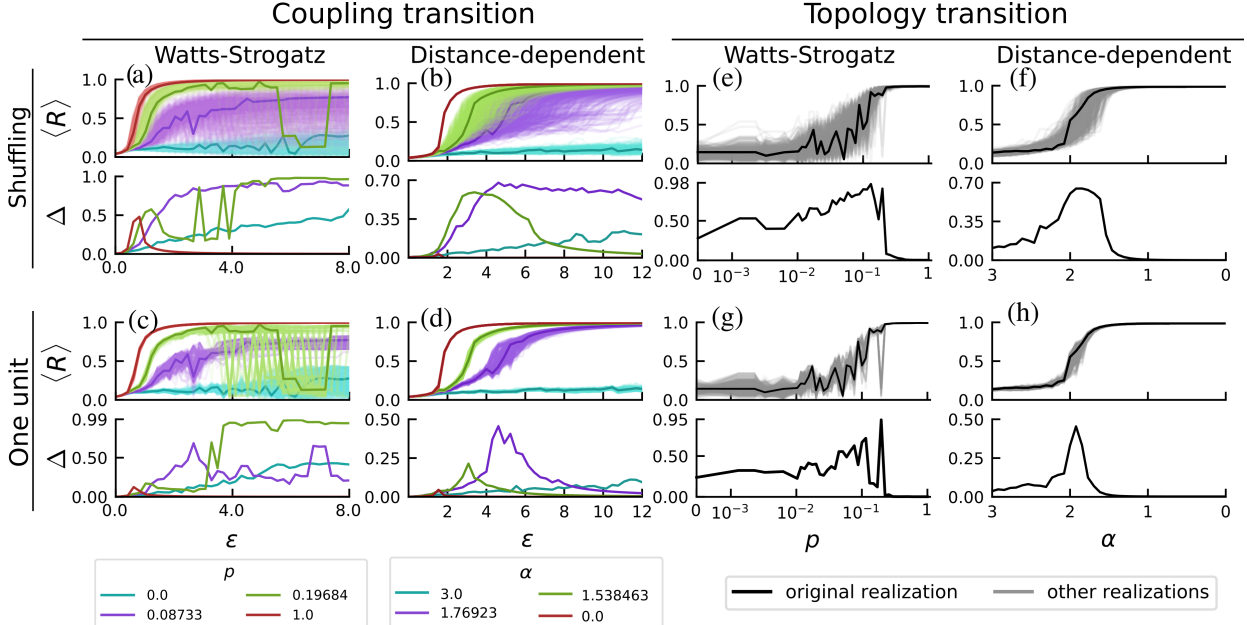


**Figure 3.3: Transitions to phase synchronization and dynamical malleability.** Networks under Watts-Strogatz (WS) and distance-dependent (DD) topologies reach phase synchronization through either an increase in coupling strength  $\epsilon$  (given the topology has a sufficient amount of long-range connections) or by switching short-range connections to long-range. Fluctuations in the degree of phase synchronization  $R$  between samples increase during the transitions, as can be seen by the differences in the same-colored curves and by  $\Delta := R_{\max} - R_{\min}$ . Starting from a natural frequency sequence originally drawn from a Gaussian distribution (thicker lines), the other samples (thinner lines) can be generated by shuffling the natural frequencies or by switching the natural frequency of one unit to  $\omega_{\text{new}} = 3$ . For intermediate networks (purple and green curves), the increase in the fluctuations (i.e. in dynamical malleability) extends for a wide range of parameters and becomes considerably large. Each panel contains  $501 = N$  realizations, with rewiring probabilities fixed for the coupling transition, with values shown in the legend, and coupling strength fixed in the topology transition at  $\epsilon = 4.51282$  for WS and  $\epsilon = 6.46154$  for DD. The initial conditions are the same across all realizations, and are randomly distributed from 0 to  $2\pi$ . The curves of  $\Delta$  are qualitatively similar with other dispersion measures, such as standard deviation, a possible difference being that the curves may be slightly shifted, as the measures can peak at slightly different values of the control parameter. We remark that the parameter values used in the simulations were generated as described in Section 3.2 and correspond to the typical behaviors in the system.

networks in Fig. 3.4. It shows, in the  $p-\epsilon$  parameter space, the average phase synchronization across samples  $\bar{R}$  on the first panel and the dynamical malleability measured by  $\Delta$  on the second panel. Figure 3.4 provides a comprehensive view on both the coupling strength and the topology-induced transitions. The samples are realized here as shuffles, though a similar figure would be obtained by changing one unit. There is a single region of phase synchronization for sufficiently high coupling strength  $\epsilon$  and rewiring probability  $p$  (panel

(a)). Around the borders of this region, where the system is transitioning, the dynamical malleability is much higher (panel (b)). It then becomes clear that the intermediate networks (green and purple lines), are near the topology-induced transition (for instance, black line) for all  $\epsilon \gtrsim 1$ . As  $\epsilon$  increases, the networks remain near this  $p$ -transition, and so their dynamical malleability does not decrease. For the regular networks, we first note that the  $p$ -axis is shown on a logarithmic scale, such that these networks, with  $p = 0$ , are still relatively close to the transition at  $p_c \approx 0.1$ , and thus they also present significant malleability.

Figure 3.4 also illustrates the existence of two qualitatively different types of transitions: one induced by increasing coupling strength (for sufficiently high  $p$ ), and another induced by increasing  $p$  (for sufficiently high  $\epsilon$ ). The difference between both is in their starting points. Both are globally phase desynchronized, but in the former (red, green, and purple lines), the weak coupling strength regimes have mostly uncorrelated oscillators, with no discernible structures in the phases or even synchronization in the frequencies. In the latter (black line), there are shorter-range structures with frequency synchronization for most samples.

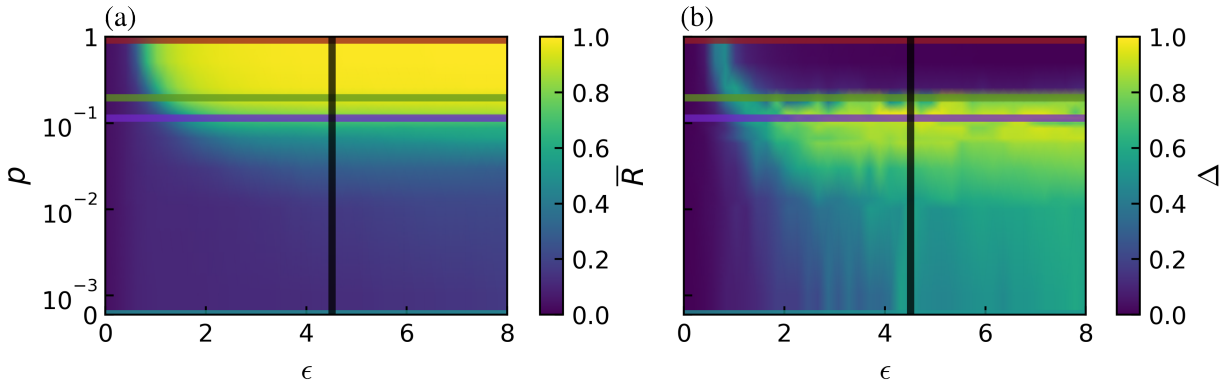


**Figure 3.4: Dynamical malleability increases around the regions of transition to phase synchronization.** The surface on the left shows the average degree of phase synchronization  $\bar{R}$  across the ensemble (1000 realizations of shuffled natural frequencies). The region of high phase synchronization is clearly seen for sufficiently high coupling strength  $\epsilon$  and rewiring probability  $p$ . The colored lines correspond to the parameter values shown in Fig. 3.3. The right panel displays  $\Delta$ , the difference between the most and least synchronized realizations for each pair  $(p, \epsilon)$ , and we see that the fluctuations from sample to sample increase during the transitions to phase synchronization. The green and purple curves remain close to the region of transition for all  $\epsilon \gtrsim 1$ , such that their fluctuations do not decrease with an increase in  $\epsilon$ . The figure uses Gouraud interpolation to ease visualization by smoothing the curves with a linear interpolation.

### 3.3.3 Unpredictability of dynamical malleability

For Watts-Strogatz networks, samples can be generated by resampling the topology instead of changing the natural frequencies. Since they are generated by a random rewiring process, different realizations generate different networks (there is link-disorder [94]). Therefore, different samples can also be generated by resampling the network while keeping the natural

frequencies fixed. This generates a profile of dynamical malleability similar to that shown in Fig. 3.3(e), where the network was fixed and the natural frequencies were changed (see Fig. S1 for details).

Now, we wish to illustrate that no network, or natural frequency sequence, is alone responsible for leading to more, or less, synchronized states. Instead, the samples depend sensitively on both, especially in the region of large STS fluctuations. Figure 3.5(a) shows the degree of phase synchronization for different realizations of the networks and different shuffles of the natural frequencies, all for  $\epsilon = 4.51282$  and  $p = 0.08733$  with fixed initial conditions. To aid the visualization, red rectangles indicate the network with the largest  $R$  for each shuffle. No network synchronizes more (or less) for any sequence of natural frequencies; and no sequence of natural frequencies synchronizes more for any network. Furthermore, if the  $\epsilon$ ,  $p$ , or initial condition are changed, the whole profile of the figure also changes. Another way to illustrate the complicated sensitivity in the region of high sample-to-sample

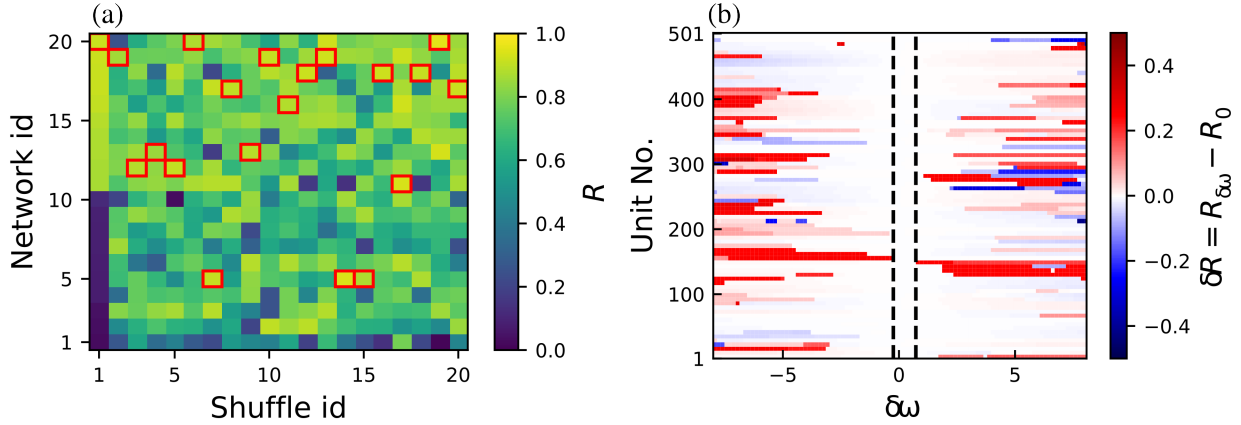


**Figure 3.5: Fluctuations in dynamically malleable systems are unpredictable.** Panel (a) shows the average phase synchronization  $R$  for fixed coupling strength  $\epsilon = 4.51282$  and rewiring probability  $p = 0.08733$  for different 20 shuffles of the natural frequencies  $\{\omega_i\}$  and samples of networks generated by the Watts-Strogatz algorithm. For ease of visualization, the networks are ordered such that the highest network ids correspond to higher synchronization for Shuffle id = 1. For each shuffle, the network with the highest  $R$  is marked with a red rectangle. We thus see that no network synchronizes more for all shuffles:  $R$  is a function of both the specific frequency and topology samples. Panel (b) shows the changes  $\delta R$  in the phase synchronization  $R$  when the natural frequency of each unit is changed by an amount  $\delta\omega$ , such that  $\omega_i \rightarrow \omega_i + \delta\omega$ . Other parameters are fixed, in particular  $p = 0.1145$  and  $\epsilon = 4.51282$ . There is a rough threshold (indicated by the black dashed lines), below which changing  $\omega_i$  does not significantly alter  $R$  ( $\delta R < 0.1$  for the figure). Furthermore, changing the frequency does not have a monotonic impact on the change in  $R$ : small alterations in  $\omega_i$ , above the threshold, can have the same impact on  $R$  as bigger alterations.

fluctuations is by now fixing the network, and changing the frequency of a single unit by an amount  $\delta\omega$ . Fig. 3.5(b) illustrates the change  $\delta R$  in the phase synchronization, compared to the synchronization of the "original" ( $\delta\omega = 0$ ) frequency realization. There is a rough threshold, at  $|\delta\omega| \gtrsim 0.1$ , below which perturbations in one unit do not significantly affect the

network's phase synchronization. Above this threshold, however, large changes occur. They are asymmetric on  $\delta\omega$  and occur non-monotonically (increasing  $|\delta\omega|$  does not necessarily lead to bigger changes). This complicated pattern we observe could make the design and control of these systems quite difficult in practice.

### 3.3.4 Ratio of short to long-range connections

As we have seen, the rewiring of connections in WS networks, or the redistribution of weights in DD networks, from short-range to long-range connections leads to a transition towards globally phase-synchronized regimes. During these transitions, the dynamical malleability peaks for some ratio of short-range to long-range connections. To quantify this ratio, we first define the short-range connections to/from a node  $i$  as all existing connections to/from other nodes  $j$  within an edge distance  $d$  (with index  $j \in [i-d, i+d]$ ), with  $d$  being the range of short connections ( $d = 2$  here). For WS networks, we calculate the average degree (number of connections) for short-range ( $K_s$ ) and long-range connections ( $K_l$ ). For DD networks, we define an analogous measure of topological influence, which is:

$$K_s := \frac{2}{\eta(\alpha)} \sum_{j=1}^d \frac{1}{j^\alpha} \quad (3.4)$$

$$K_l := \frac{2}{\eta(\alpha)} \sum_{j=d+1}^{N'} \frac{1}{j^\alpha}. \quad (3.5)$$

Note that due to the symmetry of the DD networks, nodes share the same value of  $K_s$  and of  $K_l$ . The ratio  $\kappa$  of short-range to long-range connections is then defined as:

$$\kappa := \frac{K_s - K_l}{K_s + K_l}, \quad (3.6)$$

so that  $\kappa = 1$  if only short-range connections exist, and  $\kappa = -1$  if only long-range connections exist, with intermediate cases in between. In WS networks, the number of connections is  $K = kN$  ( $k$  being the amount of neighbors of each node), with the number of long connections approximately  $K_l = pK$  and short-range approximately  $K_s = (1-p)K$ . Therefore, the ratio  $\kappa$  can be easily calculated to be approximately  $\kappa = 1 - 2p$ . For DD networks, the ratio  $\kappa$  is given as

$$\kappa = \frac{\sum_{i=1}^d i^{-\alpha} - \sum_{i=d+1}^{N'} i^{-\alpha}}{\sum_{i=1}^{N'} i^{-\alpha}}. \quad (3.7)$$

Figure 3.6 shows this ratio  $\kappa$  calculated for the same setup of Fig. 3.3(e) and (f), shuffling natural frequencies with fixed coupling strength and changing  $p$  or  $\alpha$ . The dynamical malleability is measured here by standard deviation  $\chi$  across the samples, instead of  $\Delta$ . The former makes the figure clearer, but the same analysis also works using  $\Delta$ . A remark when comparing with Fig. 3.3 is that the two measures may peak at slightly different values of  $p$  or  $\alpha$ . For both types of networks, the malleability peaks when there is a relatively small number of long-range connections present in a short-range-dominated network. It is more extreme for WS, as the ratios are closer to 1 than in the DD networks. This discrepancy in the ratios leading to higher malleability shows that  $\kappa$  is not an universal feature for any topology, but can still be important to understand their behavior.

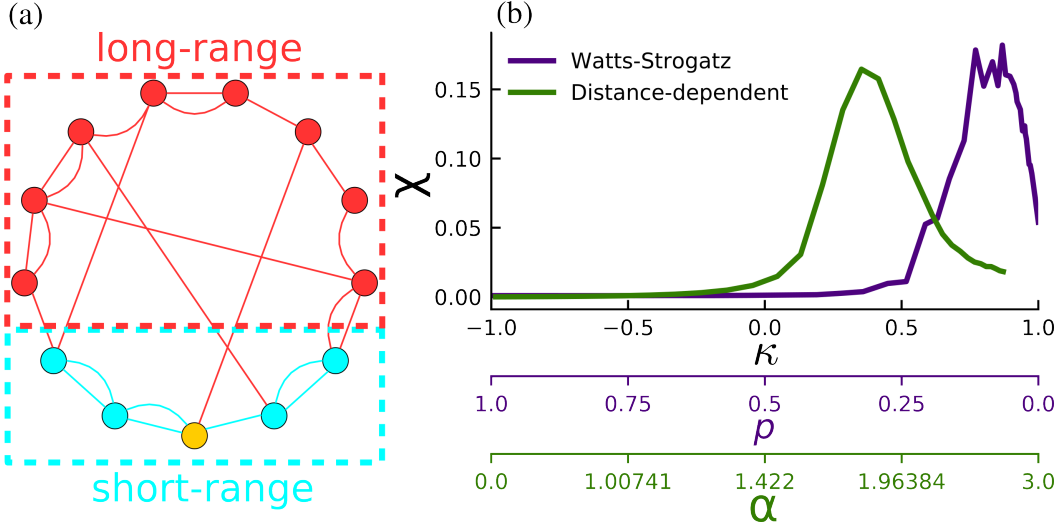


Figure 3.6: **Dynamical malleability peaks within a narrow interval in the relation of short-range to long-range connections.** Panel (a) illustrates the short-range (blue) and long-range (red) connections from the yellow unit for  $d = 2$ . Panel (b) shows the sample-to-sample fluctuations in the phase synchronization measured as the standard deviation  $\chi$  of the distribution function of  $R$  against the ratio  $\kappa$  of short-range to long-range connections calculated for several distinct topologies  $p$  and  $\alpha$ . The green curve corresponds to the distance-dependent networks, with  $\epsilon = 6.46154$  and 501 realizations per  $\alpha$ ; purple corresponds to Watts-Strogatz networks,  $\epsilon = 4.51282$  and 1501 realizations per  $p$ . The bottom axis show the values of  $p$  and  $\alpha$  for the respective ticks in  $\kappa$  (note that values of  $\alpha$  are not equally spaced).

### 3.3.5 Multistability

So far, we have changed natural frequencies while keeping initial conditions fixed. Now we invert this, and shuffle initial conditions to study the system’s multistability. We continue examining phase synchronization (PS)  $R$ , although we know that  $R$  is only a rough measure of multistability. Being a mean value, the same  $R$  could represent different attractors. Therefore, the number of attractors estimated based on  $R$  can only be considered as a lower bound. To remedy this, we also verified the findings by comparing several other features of the dynamics. These included the standard deviation of PS in time, the PS between each unit and its neighbors, the PS between sections of 100 units, the time-averaged instantaneous frequencies  $\dot{\theta}_i$  of units, and the standard deviation, inter-quartile interval and gap between the unit’s instantaneous frequencies. Realizations with unique values of all these features were considered as a distinct attractor. The number of such attractors agrees qualitatively with the dispersion we see in  $R$ , increasing during the transition.

The phase synchronization is thus shown in Fig. 3.7. Random networks ( $p = 1$ , red) are multistable only during their transition to phase synchronization. Intermediate networks ( $p = 0.19684$ , green;  $p = 0.08733$ , purple) have a high degree of multistability, meaning coexistence of several attractors, with very distinct degrees of phase synchronization. No shuffle of the initial conditions leads here to the same attractor, so the system has at least

501 attractors, the number of different realizations tested. The 2-nearest-neighbor lattice has significant multistability for  $\epsilon \gtrsim 4$ . This is consistent with the literature for 1-nearest-neighbors, in which multistability occurs after the transition to phase-locking [200].

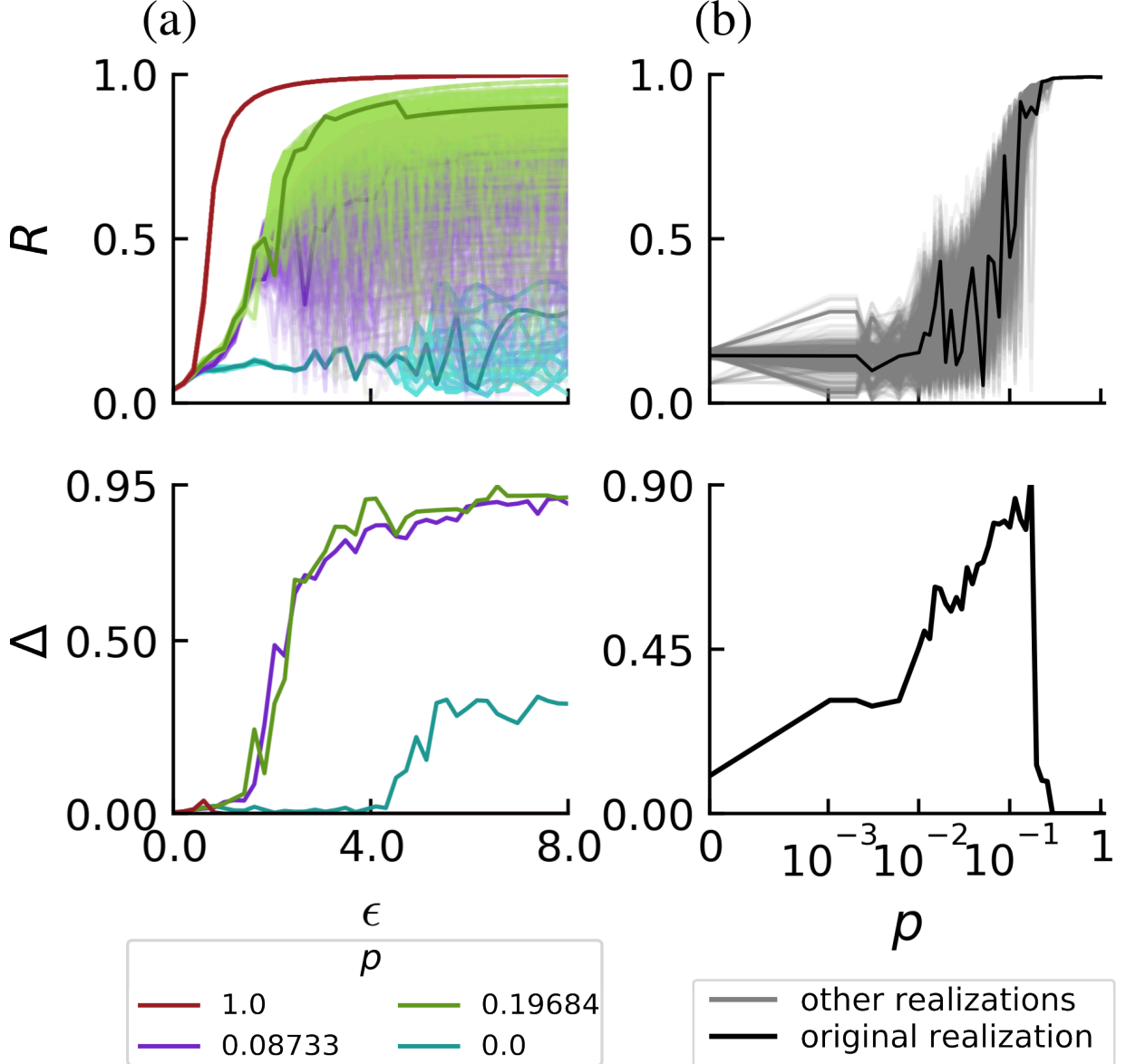


**Figure 3.7: Multistability in WS networks.** Phase synchronization and its dispersion for 501 different shuffles (thinner lines) of the initial conditions, taken from the original initial conditions (thicker lines) used throughout the rest of this work. All other parameters are fixed, including the natural frequencies as the original frequency distribution. The coupling strength  $\epsilon$  (left panel) and rewiring probabilities  $p$  (right panel) are the same ones used for WS networks in Fig. 3.3. The multistable behavior is thus very similar to what we observed before by changing the frequencies (Fig. 3.3(a) and (e)), and so shuffling the initial conditions for this network also leads to large fluctuations in the phase synchronization.

This multistability can enhance the sensitivity of the system to parameter changes, and

help to explain the large fluctuations we observe. In this case, a parameter change needs only to change the boundaries of the basins of attraction for the same initial condition to land on a completely different attractor. Attractors do not have to be necessarily drastically changed for the large dynamical malleability to be observed. However, multistability is not in principle required for STS fluctuations; in fact, the distance-dependent networks appear to be monostable (not shown), though they are malleable.

### 3.3.6 Distributions of samples

As we have seen, shuffling initial conditions can also generate realizations with widely different dynamics, similarly to shuffling natural frequencies. But the two methods to create an ensemble of samples have different effects, and can generate samples with distinct distributions. As shown in Fig. 3.8 for Watts-Strogatz networks, shuffling frequencies leads usually to a broader, and smoother, distribution of  $R$ . This increased broadness shows that new attractors are indeed created by shuffling the frequencies, so that multistability itself cannot account for the dynamical malleability we discussed previously. Furthermore, the transitions to phase synchronization occur through an increase in the distribution's average. The accompanying increase in the width of the distribution shows an increase in dynamical malleability, which goes to zero only for long-range networks ( $p = 1$ ).

Specifically, the distributions for the two-nearest-neighbor lattice ( $p = 0$ , panels (a)-(e)) are quite different: shuffling frequencies leads to a smooth distribution, whose average shifts to the right as  $\epsilon$  is increased; for shuffling initial conditions there is also a slight increase in the distribution's average as  $\epsilon$  is increased, but the distribution itself is dominated by several peaks. For intermediate networks ( $p = 0.08733$  and  $p = 0.19684$ , panels (f)-(o)), the skewness of the distribution becomes negative, and shuffling initial conditions has a smoother behavior, more similar to shuffling frequencies. Interestingly, the distribution can be bi-modal, with the two modes being separated on either extreme of  $R$  (panels (n) and (o)). For  $p = 1$  (random network), the two first coupling strengths (panels (p)-(q)) occur during the narrow interval of significant malleability, during the transition to phase synchronization. Soon after  $\epsilon > \epsilon_c \approx 1.6$ , the distribution becomes extremely narrow.

It is worth mentioning that very similar distributions are obtained if, instead of shuffling the frequencies or initial conditions, we re-sample them from the distribution (i.e. change the seed in the random number generator). Interestingly, the distributions are not Gaussian, which is inconsistent with the assumptions made in other works [91, 94]. In these works, the authors argue that the fluctuations must be normally distributed for sufficiently large networks and many samples due to the central limit theorem. This inconsistency is likely generated by the finite size of the networks studied here. Even in all-to-all networks, in which there is no topological disorder, the distributions are not Gaussian for  $N = 501$ . Results (not shown) indicate that the distributions approach Gaussian distributions as  $N$  is increased to 5000.

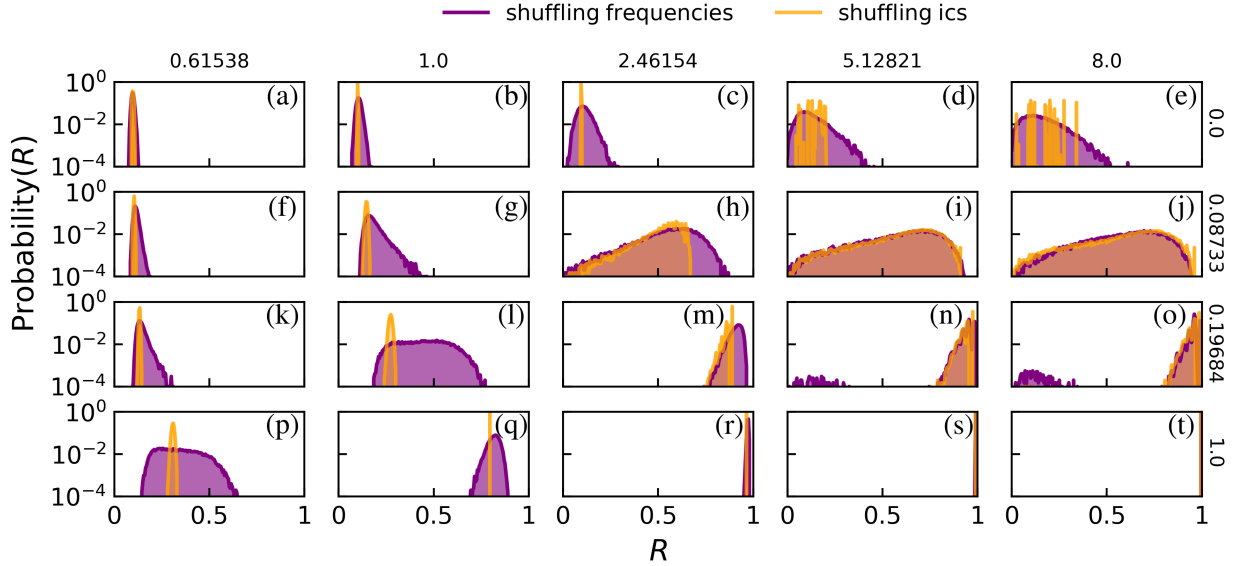


Figure 3.8: **Distributions of  $R$  due to shuffling frequencies or initial conditions.** Each panel contains the distribution of the mean degree of phase synchronization  $R$  across 20000 shuffles of natural frequencies (in purple) or initial conditions (orange) for Watts-Strogatz networks. The rewiring probabilities  $p$  are indicated on the right of each row, and are the same as used in Fig. 3.3(a); the coupling strengths  $\epsilon$  are indicated on the top of each column. Bin size is 0.005, and the probability for each bin is calculated as the occupation of the bin divided by the total occupation across all bins, and is shown in logarithmic scale.

## 3.4 Discussions and conclusions

### 3.4.1 Summary

In this work, we have studied the sensitivity of networks to changes in their units' parameters or connections, which we call their dynamical malleability, and showed that, near transitions to phase synchronization, this behavior acquires (i) a large magnitude, as changes to single units can radically alter the spatiotemporal dynamics, and (ii) a complicated sensitivity, as no analytical method we have tried was able to satisfactorily describe the changes to the dynamics. Parts of this behavior have been observed in isolation previously [31, 197, 90, 158, 12, 30] but this is, to the best of our knowledge, the first work to focus specifically on it and show its full phenomenology.

To study this concretely, we have chosen ring networks of Kuramoto phase oscillators and connected the units in two distinct classes of topology, Watts-Strogatz (WS) and distance-dependent (DD). We have either changed the frequency of a single unit or changed the frequencies of all units by shuffling (i.e., redistributing) the values of the frequencies across units. The first has allowed us to verify the impact of relatively small changes, which are still not small enough to be described in the linear regime; the latter allowed us to verify the impact of redistributing the values in the network while keeping the distribution of

parameters exactly the same, which is helpful for identifying mechanisms for the fluctuations.

### 3.4.2 Mechanisms for dynamical malleability

The two classes of topology we used have different characteristics (see Sec. 3.2) but are similar in that they lead to networks that have two distinct types of transition to phase synchronization: one induced by increasing the coupling strength and another by increasing the dominance of long-range connections. They also have differences, mostly notably that (i) the WS networks acquire a large number of attractors during their transitions to phase synchronization (i.e. become highly multistable), while the DD networks remain with one main attractor (and possibly other attractors that would have very small basins of attraction), and that (ii) the WS networks have a larger magnitude of dynamical malleability. We believe that this larger magnitude is caused by two effects: the increased number of attractors and the topology's link-disorder.

Firstly, we remark that the dynamical malleability is manifested in the networks' transitions to phase synchronization in two distinct ways. The first is through diverse onsets of the transition, as different realizations start their transitions at different values of the control parameter. This is the well-known blurriness of phase transitions described in studies of finite-size effects [25, 23]. This effect is clearly present in both networks (see, e.g., Fig. 3.3(a) and (b)). The second manifestation of malleability is in the post-transition fluctuations, i.e., in the sudden changes of synchronization that occur after the network has seemingly transitioned to synchronization (see, e.g. Figs. 3.3(a) and (c)). This effect is present here mostly in the WS networks, but is also known in other systems of finite size (see, e.g. Figs. S5(b) and (d) for the case of cellular automata). It is caused at least partly by the system's multistability, as increasing the parameter can change the shape of the attractors' basins of attraction, making the same initial condition suddenly go to another attractor. So the WS networks, which have a much larger number of attractors, exhibit this additional effect that increases their malleability, while the DD networks do not.

We further remark that multistability could have an even more pronounced impact on malleability if the basins of attraction were complexly interwoven. Then, even very small changes could lead to significant fluctuations. But this does not appear to be the case in any of the networks we studied, all of which seem to have smooth basin boundaries (Fig. S4) - it is thus noteworthy that the already high dynamical malleability we have described can occur even with smooth basin boundaries. It can even occur in the absence of multistability, as seen in the DD networks.

The second mechanism for the increased malleability in WS networks is their link-disorder [94]: different realizations lead to different topologies for a same parameter, and we observe a very similar phenomenology by comparing different realizations of these topologies (Fig. S1). This is a source of disorder, and thus, of fluctuations, that is not present in the DD networks.

### 3.4.3 Mechanisms for the fluctuations

As we have mentioned, the fluctuations in the malleable networks are also hard to predict. The behavior of the systems is clearly a complicated function that involves the coupling

strength, topology, natural frequencies, and initial conditions all together. For instance, we have not found a sequence of frequencies, or a specific network realization, that always leads to more (or less) synchronized networks (Fig. 3.5(a)). Even for fixed frequencies and topology, the most phase synchronized realization changes depend on the initial condition or the coupling strength. Changes in the natural frequency of single units also lead to non-monotonic changes in the network's phase synchronization: the change in frequency can either increase or decrease the synchronization level, depending on the chosen unit, coupling strength, and topology (Fig. 3.5(b)).

As a consequence, we are unable to identify a specific unit, or magnitude of perturbation, that is always responsible for the greatest disruption. That is, no available theory in the literature that we have tried revealed a mechanism for the fluctuations capable of predicting them. This is a surprising result, considering the quality of the available theories, the amount of research and important advancements in the description of networks similar to the ones studied here [158, 189, 26, 40]. We believe that this is mainly caused by the networks' multistability, which cannot be handled by some theories, and by the wide range of synchronization patterns.

The first theory we tried is the synchrony alignment function, which depends on the topology and natural frequencies and was shown analytically to be related to the degree of phase synchronization in the limit of strong synchrony [189]. It does not work satisfactorily for any dynamically malleable network that we tested. One reason for this is the weak phase synchronization in some realizations, which breaks the assumption of the method. Another, even stronger, reason is that our networks are multistable, such that the relation between the synchrony alignment function and the degree of phase synchronization given by the method cannot be satisfied for all attractors of the system. Indeed, it only worked perfectly in the strongly phase synchronized regime, which is also monostable.

The second theory we tried is due to Peter and Pikovsky [158], who showed in all-to-all networks that different realizations of the natural frequencies synchronize differently depending on the kurtosis of the distribution. This mechanism cannot even be expected to work for the shuffling scenarios we study since they conserve the frequency distributions and thus the kurtosis as well, but we have verified that it also does not work when the units' frequencies are changed. An additional reason why this does not seem to apply in our systems may be in the topologies, which are not all-to-all.

Thirdly, we have tested other measures that have been observed in the literature to correlate to phase synchronization, and they do not work in the malleable networks. These are: (i) the proportion  $p_-$  of links connecting nodes with natural frequencies of different signs [26]; (ii) the correlation  $c_\omega$  between the oscillators' natural frequencies, taking into account the connectivity of the network [26, 40]; (iii) the correlation between natural frequencies and the node's number of connections [189]; and (iv) the correlation between the average frequency between neighbors of a node and the node's own frequency [36, 189]. These results also cannot be expected to work in multistable networks, and indeed did not work in our networks.

### 3.4.4 Relation to statistical physics and scaling

As noted previously, there is a relation between our dynamical study here and studies on the statistical physics of networks. The transitions to phase synchronization that we see correspond to non-equilibrium phase transitions [121, 158], such that we can connect the dynamical malleability we analyze with the well-known sample-to-sample (STS) fluctuations in statistical physics. These are usually described in finite systems, in which different samples have different statistical properties that lead to distinct phase transitions - the transitions are usually said to be shifted between samples [190, 93, 91], which is one of the mechanisms we described for the malleability. As seen in these studies, the size  $N$  of the system (i.e. the number of nodes) influences the magnitude of the dynamical malleability as well as the interval of parameters in which it occurs. The networks we have presented in the results have  $N = 501$  oscillators, and scaling analysis (Fig. S2) reveals that the intervals of high malleability decrease with the size  $N$ , as expected from other studies. For instance, authors in [91] describe the range of  $\epsilon$  for high malleability as scaling with  $N^{-2/5}$  for all-to-all networks.

For the WS networks, malleability is still significant for even up  $N = 5000$  oscillators. Moreover, the maximum magnitude of the fluctuations does not decrease significantly, and networks with  $N = 5000$  can still reach  $\Delta = 0.9$ . This suggests that the malleability gets restricted to a smaller region in parameter space, but might not decrease significantly in magnitude for bigger networks. In the limit of infinite-size networks, it would get restricted to a single line, defining the two types of transitions to phase synchronization, and remain non-zero there. This is consistent with a study in all-to-all networks of Kuramoto oscillators, where this behavior was observed [92]. In fact, this behavior is well-known for phase transitions with quenched disorder (heterogeneous parameters), when systems are said to be non-self-averaging [219]. In any case, networks of  $N = 5000$  units can be regarded as rather large in several real-world applications [158], so the STS fluctuations we describe here occur for a significant range of system sizes.

### 3.4.5 Generality of the behavior

Additionally, we show that the increase in dynamical malleability is widespread in the parameter space of the systems. Looking at this space, spanned by coupling strength and the parameter controlling the topology, the dynamical malleability remains high over a wide parameter range around the two types of transitions to phase synchronization. In particular, networks with an intermediate amount of long-range connections are highly malleable for any coupling strength  $\epsilon$  we tested (e.g. green and purple lines in Fig. 3.3). This is because the topology is fixed, so the networks remain close to the topology-induced-transition even though they are far from the coupling-strength-induced-transition.

We also remark that the phenomenology we describe also occurs for wide ranges of topology and coupling strength values, for distinct frequency distributions, such as Cauchy-Lorenz (not shown), and for other dynamical models. For instance, previous works on spiking [31] and bursting [30] neural networks have revealed a very similar phenomenology. We also show similar behavior for cellular automata (see Fig. S5). We have observed (not shown) similar behavior in small-world networks generated by adding long-range connections and keeping the short-range ones [152]. Other works have also observed dynamical malleabil-

ity in Kuramoto oscillators coupled under both human-connectome structural networks and hierarchical-modular networks [34, 212]. Additionally, of course, the theory of phase transitions and, consequently, of sample-to-sample fluctuations is known to apply for a variety of distinct systems.

### 3.4.6 Practical importance of malleability

The discussions lead to an interesting question: is dynamical malleability good or bad? On the one hand, large fluctuations can be undesired. For instance, a large fluctuation could take power grids from a phase synchronized regime to a desynchronized one, and lead to blackouts. On the other hand, fluctuations can be desired due to the increased flexibility in the systems. They could be a useful mechanism for adaptation, learning or memory formation in neural circuits. More specifically, an important property of the brain is that it can separately process information from different types of input in segregated areas, and then integrate them all into a unified representation [203, 204, 53]. For this reason, Tononi and colleagues conjectured that the brain needs to have an optimal balance between segregation and integration of areas [203]. In this optimal balance, the synchronization between different brain regions needs to fluctuate from low synchronization to high synchronization [62]. Therefore, having a large dynamical malleability can be an advantageous feature, allowing for this high variability to be achieved through small changes in the neurons, e.g. their firing rate, or their connections. There is also interesting evidence for this in [128], which reported that high-frequency firing of neurons can drive changes in the global brain state.

### 3.4.7 Future research and conclusions

An interesting line of research opened here is to understand ways to quench or to explore the fluctuations between realizations, using the framework we establish here, for practical applications. Another interesting line of research is to consider the effects of noise or time-dependent forcing on malleable systems: since they have a wider range of dynamical states available by changing parameters, a time-dependent change in the parameters, induced by the noise or forcing, can lead to transitions between several different states. The complicated and sensitive dependence on the parameters would mean that even small amplitude changes could lead to drastic fluctuations. For the Watts-Strogatz networks, multistability can complicate the dependence on external inputs, and make the effects dependent on the timing of perturbations, as different states, all of which coexist, can react differently to the parameter changes. Understanding these behaviors is important, for instance, in the context of neural systems, where external influences are common and where temporal fluctuations are essential.

Future research is also needed to fully describe the mechanism for the fluctuations between realizations. An interesting possibility could be to extend the synchrony alignment function [189] to weakly synchronized regimes or to multistable systems. Another promising approach would also be to apply the formalism introduced in [146, 33]. A third possibility would also be to use the model reduction method by [82]. These would be important theoretical contributions for the understanding of phase synchronization in oscillator networks and for the role of each unit in a network.

To summarize, the increased magnitude and complexity of dynamical malleability shown here is a general phenomenon in finite-size systems that can be expected to occur in real-world systems.

## Acknowledgments

We would like to thank Jan Freund and Arkady Pikovsky for helpful discussions. K.L.R. was supported by the German Academic Exchange Service (DAAD). R.C.B. and L.E.M. acknowledge the support by BrainsCAN at Western University through the Canada First Research Excellence Fund (CFREF), the NSF through a NeuroNex award (#2015276), SPIRITS 2020 of Kyoto University, Compute Ontario ([computeontario.ca](http://computeontario.ca)), Compute Canada ([compute-canada.ca](http://compute-canada.ca)), and the Western Academy for Advanced Research. R.C.B gratefully acknowledges the Western Institute for Neuroscience Clinical Research Postdoctoral Fellowship. B. R. R. B. acknowledges the financial support of the São Paulo Research Foundation (FAPESP, Brazil) Grants Nos. 2018/03211-6 and 2021/09839-0. The simulations were performed at the HPC Cluster CARL, located at the University of Oldenburg (Germany) and funded by the DFG through its Major Research Instrumentation Program (INST 184/157-1 FUGG) and the Ministry of Science and Culture (MWK) of the Lower Saxony State, Germany.

# Chapter 4

## Dynamical properties and mechanisms of metastability: a perspective in neuroscience

Kalel L. Rossi<sup>1</sup>, Roberto C. Budzinski <sup>2,3,4</sup>, Everton S. Medeiros <sup>1</sup>, Bruno R. R. Boaretto <sup>5</sup>, Lyle E. Muller <sup>2,3,4</sup>, Ulrike Feudel<sup>1</sup>

<sup>1</sup> Theoretical Physics/Complex Systems, ICBM, Carl von Ossietzky University of Oldenburg, Oldenburg, Lower Saxony, Germany

<sup>2</sup> Department of Mathematics, Western University, London, Ontario, Canada,

<sup>3</sup> Western Institute for Neuroscience, Western University, London, Ontario, Canada,

<sup>4</sup> Western Academy for Advanced Research, Western University, London, Ontario, Canada,

<sup>5</sup> Institute of Science and Technology, Federal University of São Paulo, São José dos Campos, São Paulo, Brazil

**Abstract.** Understanding the sensitivity of a system's behavior with respect to parameter changes is essential for many applications. This sensitivity may be desired - for instance, in the brain, where a large repertoire of different dynamics, particularly different synchronization patterns, is crucial - or may be undesired - for instance, in power grids, where disruptions to synchronization may lead to blackouts. In this work, we show that networks of coupled phase oscillators with nonlinear interactions can acquire a very large and complicated sensitivity to changes made in either their units' parameters or in their connections. Even modifications made to a parameter of a single unit can radically alter the global dynamics of the network in an unpredictable manner. This occurs over a wide parameter region, around the network's transitions to phase synchronization. We argue that this is a widespread phenomenon that can be expected in real-world systems, extending even beyond networks of oscillators. Metastability, characterized by a variability of regimes in time, is a ubiquitous type of neural dynamics. It has been formulated in many different ways in the neuroscience literature, however, which may cause some confusion. In this Perspective, we discuss metastability from the point of view of dynamical systems theory. We extract from the literature a very simple but general *definition* through the concept of *metastable*

*regimes* as long-lived but transient epochs of activity with unique dynamical properties. This definition serves as an umbrella term that encompasses formulations from other works, and readily connects to concepts from dynamical systems theory. This allows us to examine general dynamical properties of metastable regimes, propose in a didactic manner several *dynamics-based mechanisms* that generate them, and discuss a theoretical tool to characterize them quantitatively. This perspective leads to insights that help to address issues debated in the literature and also suggest pathways for future research.

## 4.1 Introduction

Time-series of neural activity often reveal series of transitions between experimentally observable regimes with unique dynamical properties. For example, as subjects fall asleep, their brains progress through a series of well-defined patterns, from the 11-15 Hz sleep spindle [44], to the large low-frequency rhythms of deep sleep [191], and to waking-like activity during rapid eye movement (REM) sleep [107]. These sleep stages, or regimes, can also occur on shorter timescales, as subjects transition from passive rest to active perception [165]. This ubiquitous phenomenon of regime switching has prompted connections to the concept of *metastability* in physics and dynamical systems theory. Many works have demonstrated metastability in neural systems across different spatiotemporal scales and species [144, 211, 127, 105, 39, 137, 172, 28, 1, 186, 104, 131, 136, 185, 135, 54, 97, 202, 164, 47, 58, 42, 125].

Understanding the mechanisms based on dynamical systems theory that can generate such metastable regimes is crucial, especially as this knowledge can aid in the development of techniques to predict transitions between regimes and to possibly control them. The literature in neuroscience has made crucial advancements in this regard [202, 64, 78, 43, 28, 65, 51], but differences in formulation between works can lead to some confusion. For instance, the explicit definition of metastability is not totally clear in the neuroscience literature (see Sec. 4.2.2 for more). Further, discussions on the dynamics-based mechanisms for metastability are usually restricted to only a few possible mechanisms, depending on the context and formulation of each work.

In this Perspective, we aim to address these issues by discussing the neuroscience literature through the lens of dynamical systems theory. First, we extract from the literature a very simple but general definition of metastability, based on *metastable regimes*. Regimes are epochs of a time-series identified in each work that have unique dynamical properties. They are considered metastable when they are *long-lived but transient*. This idea is widespread among works not only in neuroscience, but is also similar to the well-defined view in physics and dynamical systems theory [155, 38, 221]. The characterization as long-lived is specific to the system being studied, and discussed in details later. We argue that all metastable regimes share a crucial defining property in state space, which is the space spanned by all variables of a system (explained in detail in Sec. 4.3.1). Simply put, metastable *regimes* correspond to metastable *regions* in state space, in which trajectories have a high probability of remaining inside. This idea can be formulated theoretically through the concept of almost-invariant regions [71, 55] (see Sec. 4.3.2 for details).

Associating metastable regimes in time to metastable regions in state space, which in turn

are defined as almost-invariant [71, 55], allows for a single coherent view on metastability. It also allows for a direct connection to well-known dynamics-based mechanisms from dynamical systems theory. Here, we discuss and compare several of these mechanisms in a didactic manner. By looking into them together through a general definition, we are able to add important insights into issues debated in the literature and propose new research directions to generate experimentally testable and falsifiable hypotheses about metastability in the brain, potentially including phenomena such as sleep, seizures, and computations in neural circuits.

## 4.2 Short summary of metastability in the brain

### 4.2.1 Observations of metastability

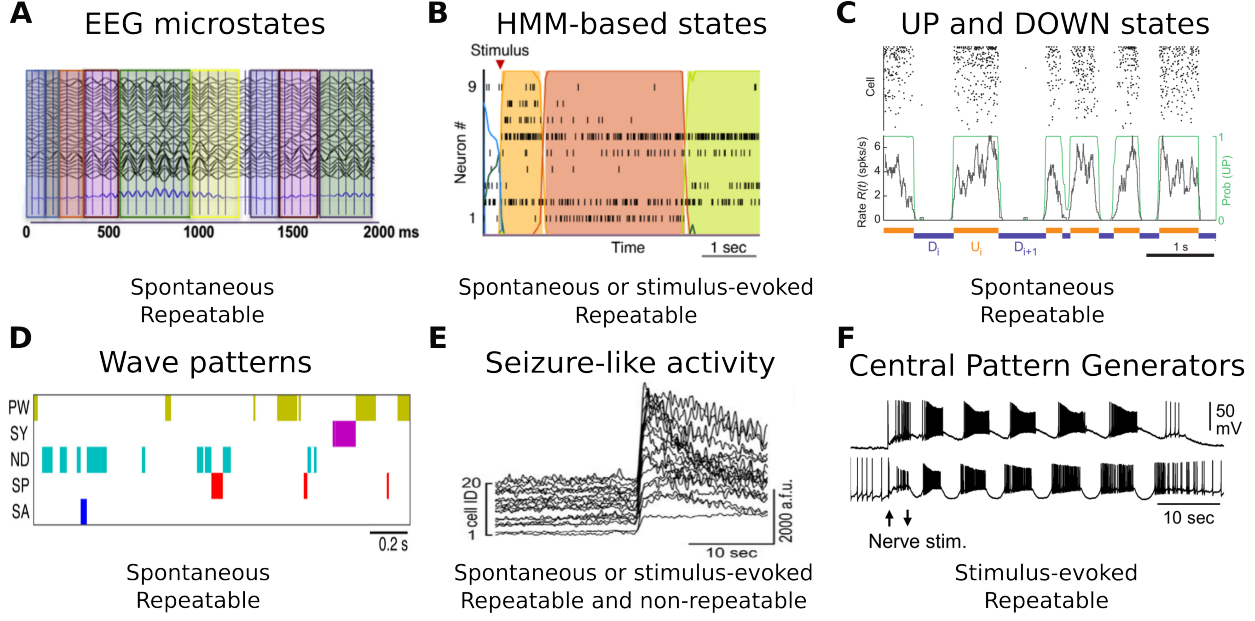
We now review key observations that have helped to establish metastability as an important dynamical phenomenon. We focus on examples of metastability characterized by the switching between long-lived regimes of activity. These regimes are epochs of observations with unique dynamical properties identified by the authors of each work, and their characterization as long-lived depends on the specific application being considered. Further, as a note of terminology, these regimes are often called states in the neuroscience literature, but we avoid this here because it conflicts with already well-established terminologies in other fields of science. Instead, we believe regime is equally descriptive, and less ambiguous. In this section, we only maintain state as a synonym for regime when it refers to a well-established name, such as EEG microstates.

Figure 4.1 illustrates some observations showing time-series with metastable regimes, along with two corresponding characteristics: (i) whether the transitions between the regimes occur during resting conditions (spontaneously) or if they are evoked by some stimulus; and (ii) whether the metastable regimes occur more than once in the observation (repeat) or not.

As a first example, Fig. 4.1A shows time-series of electroencephalography (EEG) measurements performed in resting humans with eyes closed (taken from Ref. [144]). Colors indicate **EEG microstates**, identified from the spatial configuration of the electric potential amplitude of each electrode. These microstates remain almost constant for roughly 100 ms [211, 127], and then give way to other microstates.

Figures 4.1B-C show results based on firing rates of neurons. In particular, Fig. 4.1B shows exemplary sequences of regimes adapted from Ref. [28]. The regimes are characterized by roughly stationary behavior in the firing rates of neurons in the gustatory cortex of rats, and are identified via the technique of **hidden Markov modelling** (HMM). Each regime lasts for roughly an order of magnitude longer than the transitions between any regime [105, 39, 137, 172, 28]. This is observed during both spontaneous and stimulus-evoked activity, and the sequence of such regimes is shown to encode the stimuli presented to the animals [39, 137]. These regimes are proposed to serve as a “substrate for internal computations” in the brain [39]. Similar results have also been reported in the frontal cortex of monkeys during a delayed localization task [1, 186].

Figure 4.1C shows sequences of sustained firing (significant activity, **UP states**) and



**Figure 4.1: Brain activity typically evolves as a sequence of well-defined regimes that are transient but long lived.** The panels illustrate observations taken from the literature, namely EEG microstates [144] (A), firing rate states identified via hidden-Markov-modelling (HMM) [28] (B), UP and DOWN states [104] (C), cortical wave patterns [206] (D), seizure-like activity [217] (E), and bursting in central pattern generators [184] (F). Each observation is explained in detail in the main text, and is classified into subtypes of metastability that we define in the Sec. 4.3.4.

silence (**DOWN states**) in the firing rates of the deep layers of the somatosensory cortex of urethane-anesthetized rats (adapted from Ref. [104]). Each regime lasts for a significant time, with quick transitions between them [104]. These regimes are ubiquitously observed in spontaneous activity [131, 104].

Figure 4.1D shows a sequence of complex **wave patterns** identified in the cerebral cortex of anesthetized marmoset monkeys, taken from Ref. [206]. Starting from local field potential data from multiple electrodes, the authors created a spatial map for the phases of the oscillations, filtered at the  $\delta$  band (1 – 4 Hz), from which they identified different spatiotemporal patterns, classified as plane waves (PW), synchrony (SY), node (ND), spiral (SP), and saddle (SA) [206]. These patterns repeat across the time series, but the probability of switching from one pattern to another differs from pattern to pattern, i.e., there is preferential switching between patterns [206].

Mazor and Laurent [136] (not included in the figure) measured the firing rate of neurons in the antennal lobe of locusts as the animals were presented with a variety of odor pulses. Their results suggest that, for long pulses (lasting more than 2 s), spiking activity in the antennal lobe switches between a baseline fixed point and an odor-specific fixed-point, which can last for a few seconds. Interestingly, the transition epochs between the two fixed points were found to contain the most amount of information about the stimuli, suggesting an important role for them in neural computations [136, 170]. This suggests a functional role

of transitions between metastable regimes for information processing [136, 17].

Figure 4.1E shows the neural activity recorded by two-photon calcium imaging in mouse neocortex [217] (Copyright 2019 Society for Neuroscience). The neural population is being invaded by a propagating **seizure-like activity**, which appears in the middle of the time-series, and is characterized by sustained firing of a large number of neurons. Traveling as a wave, it transiently replaces the baseline regime, in which firing is more sparse and distributed. In this study, a pharmacological agent was applied to a specific region of the cortex to induce the seizure-like activity.

Figure 4.1F shows the swim motor pattern in intracellular recordings of two neurons that belong to the swim central pattern generator of the mollusk *Tritonia* [184] (adapted from Ref. [184]). These neurons respond by **bursting** when nerve PdN3 is stimulated. These bursts are phenomenologically similar to those shown later in Fig. 4.4E (though their mechanisms might differ), and demonstrate the alternation between periods of sustained firing and periods of silence. The dynamics of central pattern generators often include metastable regimes [133].

Another work (not included in the figure) has also found that the power spectrum of local-field potential (LFP) recordings in rats progresses as a sequence of relatively stationary regimes lasting for some time before rapidly transitioning to other regimes [97] (see e.g. Fig. 2 of Ref. [97]). This was observed as the rats recovered consciousness, when the concentration of an anesthetic was progressively decreased. The authors argue that the existence of well-defined metastable regimes is crucial for the fast recovery of consciousness [97].

Additionally, we remark that several other regimes could be mentioned in this section, such as other types of seizures [47, 18]; sleep spindles [58], transient patterns of circular waves that repeatedly travel across the cortex during sleep and may aid the consolidation of memories [147], and the phases of local-field potentials in cats at rest [202, 164]. For further reviews on this topic, we refer the reader to Refs. [202, 28, 43, 207].

### 4.2.2 Current formulations of metastability

Several theoretical formulations have been employed to study the observations of metastability in the brain, but they have remained focused mostly on the specific context of their observations, and a general view is currently lacking. To illustrate this issue, we depict in Figs. 4.2A-F the main formulations of metastability that we have identified in the neuroscience literature.

We can generalize the formulations in Figs. 4.2A-E as considering metastability to be a behavior with a type of variability in the dynamics. This variability can be directly observed as different *patterns of activity* (Fig. 4.2A) [69, 70, 209, 174]; or *patterns of synchronization* (Fig. 4.2B, where activity shifts between in-phase and out-of-phase) [37, 52, 51, 163, 4]. As mentioned in the previous section, abstract regimes can be identified through techniques such as Hidden-Markov model [138, 39, 28] or Principal Component Analysis (PCA) [185]. Then, metastability is simply said to be the variability of these regimes (Fig. 4.2C, with each circle representing one distinct regime) [138, 39, 3, 6, 126, 214, 87, 148, 168, 43, 218, 22]. In other works, metastability is said to occur due to variability of trajectories along different *regions of state space* [96, 78]; see Fig. 4.2D, where the black curve represents a trajectory

passing through equilibria in colored circles, with their stable and unstable manifolds in dark green and red, respectively. For a detailed explanation of these concepts, we refer the reader to Sec. 4.3.1. Metastability has also been defined as a variability along different positions on an *energy landscape* (Fig. 4.2E) [76, 43, 4, 96]. Another, more distinct, formulation of metastability is that of a behavior with *integration-segregation*, in which neural assemblies transiently synchronize and desynchronize (Fig. 4.2F, where the nodes represent assemblies whose anatomical or functional connections correspond to lines, and their activity to colors, which alternate between synchronized and desynchronized) [53, 61, 202, 201, 27, 111, 86].

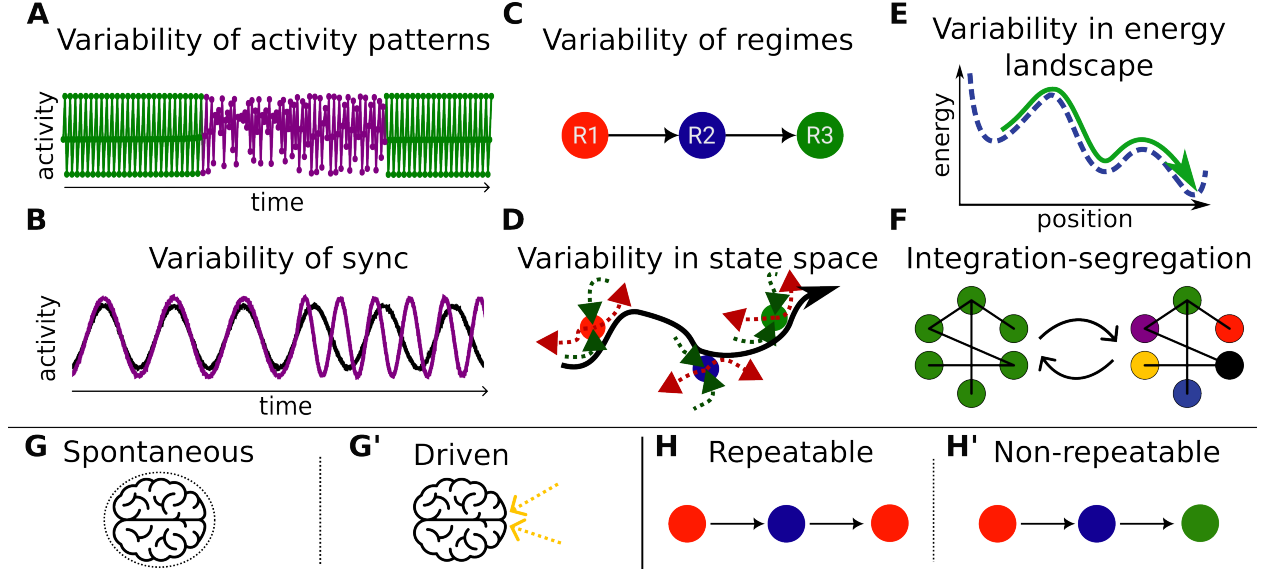


Figure 4.2: **Formulations of metastability in the neuroscience literature.** A common theme among these is the presence of transitions between certain aspects of the system’s dynamics (e.g., between activity patterns). The upper part of the figure (A-F) illustrates what these aspects are in each formulation, and the bottom part (G-H’) shows characteristics of the transitions. Further details are available in the main text.

Furthermore, we remark that, while some works explicitly mention a time-scale separation in metastability [96, 28], others do not. Works also differ in regard to the possible mechanisms giving rise to metastability. Some consider that the variability in the dynamics needs to be spontaneous, occurring in autonomous systems (Fig. 4.2G) [185, 111, 174, 63, 43], while others argue that the variability must be externally induced, occurring in non-autonomous systems (Fig. 4.2G’) [104, 96]. A combination of both is also found in Refs. [28, 70, 39]. Finally, another source of difference is in the repeatability of metastable regimes: some works consider metastable regimes only when they are repeatable (Fig. 4.2H) [78], while others also consider non-repeatable (Fig. 4.2H’) regimes [28]. Examples of these types of metastability are shown in the observations in Fig. 4.1.

### 4.2.3 The common thread

As we have seen in the previous sections, the explicit formulation of metastability can vary considerably depending on context. However, there is a common thread across all the ob-

servations and formulations. It starts with the notion of regimes as epochs of a time-series with unique dynamical properties. For instance, unique spatial configurations of the EEG electric field define unique EEG microstates [144], and UP states have an above-threshold firing rate, while DOWN states do not [104]. Further, these regimes often have constant, or almost-constant properties throughout their duration.

Then, regimes are characterized as long-lived, even if only qualitatively, establishing thus the common thread across works: **metastable regimes are long-lived but transient**. Although sometimes implicit, we believe this common thread is the fundamental aspect of metastability as a dynamical behavior. This is also the view that has been held generally in physics [155, 38].

In this Perspective, we look into dynamics-based mechanisms that generate such metastable regimes, connecting these ideas with dynamical systems theory. To achieve this, we introduce some crucial concepts from this theory in the next section.

## 4.3 Metastability in state space

### 4.3.1 Stability and invariance - initial concepts

A dynamical system is a set of  $N$  variables together with the rules that dictate their time evolution. These variables may be observables identified from experiments, for instance. At each instant, the values of these  $N$  variables define the *state*  $\mathbf{s}$  of the system. The  $N$ -dimensional abstract space containing all possible states of a system is called the *state space*. In this space, each dimension corresponds to a variable of the system.

For example, consider a ball moving in a landscape with two wells separated by a hill (cf. Fig. 4.3A). When released, the ball rolls downhill in this landscape. Appropriate variables defining the state of the ball at any given time are its position  $x$  and velocity  $v$ , such that we can write the state  $\mathbf{s}$  of the ball as a two-dimensional vector  $\mathbf{s} = (x, v)$ . So the state space for the ball will have two dimensions: one for  $x$ , another for  $v$ , as represented in Fig. 4.3A'. We can initialize this system by releasing the ball from a certain height with some speed, defining an initial state  $\mathbf{s}_0 = (x_0, v_0)$ .

This initial state, also called initial condition, is one point in state space. Once released, that ball will evolve in time, going through a continuous sequence of different states, revolving around the well until it eventually comes to rest at the bottom of one well. This sequence of states representing the movement of the ball is called a *trajectory* of the system, and corresponds to a path in state space. Equivalently, a trajectory is a set of points (a set of states). There are infinitely many trajectories in state space; one of them is represented in Fig. 4.3A' as the black curve.

Dynamical systems theory shows that the time evolution of the infinitely many trajectories is governed by the properties of certain structures present in state space. It then becomes crucial to understand these structures.

To start, notice that in the example the ball eventually converges to the bottom of one of the wells because it loses energy due to friction. In general, any system characterized by energy losses will converge to *attractors*, which are attracting sets of points in state space. The state of the ball at rest on the bottom of each well is an equilibrium attractor, as the

trajectories converge to that state and stay on it indefinitely. The equilibrium thus does not change under the time evolution of the system, and is called *invariant*. If one were to periodically kick the ball, it may start to draw a periodic motion: instead of converging to a single point, it revolves around the well and repeats its motion every certain period. In state space this corresponds to a closed loop, also an invariant set. Other invariant sets are also possible, such as chaotic sets, in which the long-term behavior of a trajectory is highly sensitive to changes in its initial conditions.

Attractors are said to be locally stable in state space: any small perturbation away from an attractor leads to a trajectory that eventually returns to it. An important remark is that this double well system has two stable equilibria, i.e. two attractors, so it is called bistable (in general, for more attractors, it would be called *multistable* [59, 60]). To which of the two attractors the ball converges depends on its initial state.

Another class of important structures are unstable sets. We have one such structure in the double well: the top of the hill. If a trajectory starts exactly on top of the hill, it will stay there for an infinitely long time; again, the top of the hill is invariant. If we perturb the ball, even slightly, it will leave the top and converge to one of the wells.

The stability of invariant sets can be understood from a geometrical point of view in state space. While the stable equilibrium attracts trajectories from all directions near it, the unstable equilibrium has specific attracting and repelling directions. In this case, the unstable equilibrium is said to be of saddle type [156], in reference to saddles (e.g. a horse-riding saddle), which also have such attracting and repelling directions. These directions are called the stable and unstable manifolds of the equilibrium, respectively. Figure 4.3A' shows the saddle equilibrium in a red circle, with its stable and unstable manifolds as green and red curves, respectively. Saddle-points, or in general saddle invariant sets, play an important role in several deterministic mechanisms leading to metastability, as we show in Sec. 4.3.3.

Before proceeding, we remark that an alternative introduction to many of these concepts is provided in Ref. [114].

### 4.3.2 Metastability and almost-invariance - definition

In the previous section we introduced a common notion of stability, which requires that a set is invariant, such that trajectories reaching it remain on it for infinitely long times. Now let us imagine a different scenario in the double well landscape: suppose the ball has a small demon that is constantly kicking it in randomly chosen directions with randomly chosen strengths, as illustrated in Fig. 4.3B. This effectively adds noise to the ball's evolution, creating a *noisy* system. The landscape of course has not changed, so the *noiseless* system is still the same. Therefore, the ball still tends to roll downhill, attracted towards the bottom. But the noise often kicks it away, repelling the ball from the bottom. As a result of this interplay between attracting and repelling tendencies, the ball is always in motion, revolving randomly around the bottom of one well, but never gets stuck to it.

Eventually, by chance, the demon will give the ball successive kicks up the hill in such a way that it overcomes the top and falls onto the other well. How many kicks are needed depends, on average, on the noise strength: lower noise requires on average more kicks, such that the ball can stay around one well for very long epochs (see Ref. [100] for more details).

So the ball with noise never converges to an attractor - instead, it moves for potentially

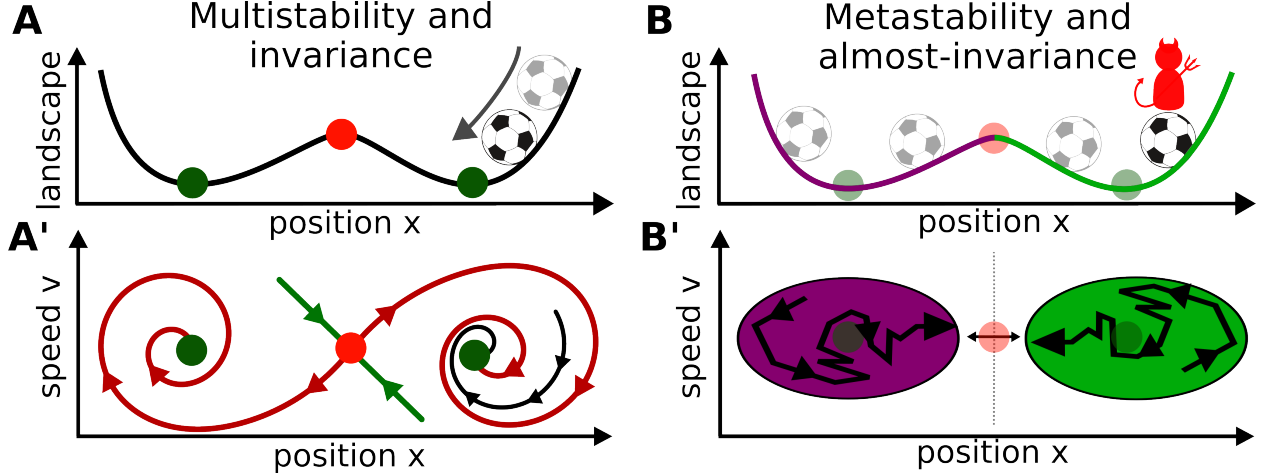


Figure 4.3: **Illustration of multistability versus metastability.** Panels A and A' illustrate the behavior of a ball on a double-well landscape, representing a multistable system. The stable and unstable equilibria are represented by green and red circles, respectively. In A, the ball is shown on the landscape to converge to the equilibrium on the right, where it stays indefinitely (equilibria are invariant). In A', a possible corresponding trajectory is shown in state space. The green curves leaving the unstable equilibrium denote its stable manifold, while the red curves denote the unstable manifold. In B, we suppose there is a demon kicking the ball and thus introducing white noise to its dynamics. This now makes the ball switch eternally between the two wells, and effectively transforms the previous equilibria (not invariant anymore, represented as faded circles) into metastable regions (which are almost-invariant), represented illustratively in B' by the purple and green ellipses.

very long times inside a region close to where the noiseless attractor is located, and eventually leaves. The noise transforms the ball's dynamics from stable equilibria into metastable regimes, *from multistability into metastability*, in the sense of long-lived but transient regimes that we discussed in Sec. 4.2.3 [100, 160, 10, 118, 116, 117, 59]. This idea is illustrated in Figs. 4.3B and B'. It should be noted that these remarks are valid as long as the noise strengths are not large enough to create purely noisy trajectories, which just diffuse through the state space.

In the noiseless system, the bottom of each well forms an invariant set. In the noisy system, we have seen that two regions emerge in which the ball spends a long time. These regions are *almost-invariant*, in the sense that trajectories inside them have a high probability of remaining inside as they evolve [71, 55]. An almost-invariant region  $R$  can be defined such that the probability of staying inside it after some time evolution is large enough that trajectories stay inside for long periods of time. The higher the probability, the longer they stay. These concepts have been nicely formalized in previous works [71, 55], so we refer the reader to those references for more details. We provide a brief summary in the Supplementary Material.

Importantly, note that noise is, in general, not necessary for generating almost-invariant regions - as we see later in Sec. 4.3.3, there are also several mechanisms that lead to almost-invariant regions in deterministic, autonomous systems. The case with noise was used here

only as a simple concrete example.

Therefore, we can say in general that a region  $R$  of state space is metastable if it is almost-invariant, that is, if trajectories, once in  $R$ , tend to stay in  $R$  for a long time before leaving. This is a key point in our Perspective: **metastability is observed through *long-lived but transient* (metastable) regimes, and underlying any metastable regime is an *almost-invariant* (metastable) region of state space.**

This view formalizes the notion of long-lived but transient regimes and reformulates them into properties in state space, associating a dynamical regime to its corresponding region, and associating that region to an interpretable quantity, namely the probability of trajectories remaining inside. The concept of almost-invariance is crucial for this, and serves as a theoretical tool to quantitatively characterize metastability.

In some applications, one might be concerned with the minimum duration of metastable regimes, i.e., how long regimes need to be in order to be metastable. This question requires an arbitrary decision on a threshold, which cannot be objectively decided in general; it depends on the specific application. The advantage of this definition is that it is agnostic to a minimum duration and thus flexible to this decision. Another advantage is that the decision can be made not in terms of a duration, but in terms of a probability, which may have a clearer interpretation.

Beyond their characterization, the identification of metastable regimes is also an important problem, which has seen several solutions in the neuroscience literature, as discussed in Sec. 4.2.1. An interesting approach is through optimization procedures that aim to maximize the probability of trajectories remaining inside the almost-invariant regions [72, 71, 55]. This can identify maximally almost-invariant regions, on which regimes will be maximally long, on average. These regions have been shown for some systems to have a particular geometrical property: they are partially separated in state space by invariant manifolds, which gives further insight into their structure and localization [74]. The technical details of how this identification can be done for observed time-series, however, go beyond the scope of this Perspective, and is the subject of ongoing research [73].

Further, it is worth remarking that metastability of a regime does not fully define its dynamics. As we see in the next section, metastable regimes can be, for instance, periodic or chaotic, generated by deterministic or by noisy mechanisms, etc. A deeper analysis is required to fully characterize metastable regimes.

### 4.3.3 Dynamics-based mechanisms for metastability

The definition of metastability encompasses the observations and formulations previously reported in neuroscience. Furthermore, and crucially, it also allows one to study concrete mechanisms that generate metastable dynamics. These are known from dynamical systems theory. Some have been proposed in the context of metastability [78, 43, 28], but others have not yet so far, to our knowledge.

Before we proceed to the mechanisms, we remark that around any metastable region there is a *coexistence of attracting and repelling tendencies* [202, 109]. The ability of metastable regions to retain trajectories is due to their attracting tendencies, and their finite duration is due to their repelling tendencies that push the trajectories away - for instance, in the double-well example, think of the attraction towards either of the two wells versus the repulsion due

to the noise.

The double-well landscape with noise is a simple example of the general behavior of **noise in a multistable system**. As we have discussed before, trajectories spend considerable time around one well, then hop to the other well, and repeat this behavior indefinitely. This phenomenon is called *attractor hopping* [116]: the system now has two metastable regimes, each corresponding to the dynamics around one well. In this sense, *noise replaces the stable equilibria with metastable regions*. The regimes can be seen in the time-series of the ball's position  $x$  in Fig. 4.4A and the regions in the ball's state space, spanned by its position  $x$  and velocity  $v$ , shown in Fig. 4.4A'. The times spent on each metastable region (called residence times or dwell times) follow a probability distribution, such as an exponential distribution for Gaussian white noise [83] (Fig. 4.4A''). This mechanism of noise-induced transitions in multistable systems has been proposed for several observations of metastability in the brain [28, 96].

We introduced metastability with the example of a noisy system in Figs. 4.3B-B' and 4.4A-A'', but metastability can also occur without any noise or external input, due to several possible *deterministic* mechanisms. We concentrate now on some of these, starting with a **stable heteroclinic cycle**, which is demonstrated here by a firing-rate model derived from three synaptically-coupled Hodgkin-Huxley neurons [16]. Figure 4.4B shows the time-series of a trajectory on such a cycle, performing a sequential alternation between three distinct regimes, each with a unique color. These regimes correspond to the vicinity of specific points in state space, as highlighted in Fig. 4.4B'. They are saddle-points, like the red circle shown in Figs. 4.3A-A', which have coexisting attracting directions (stable manifold) and repelling directions (unstable manifold). The stable manifold of one saddle is connected to the unstable manifold of the next, in what is called a heteroclinic connection [156]. Furthermore, this cycle is stable: trajectories approach one of the saddle-points along its stable manifold and potentially spend a long time near it - then, they depart along its unstable manifold to the next saddle, and so keep cycling through them, converging ever closer to the saddles and their manifolds. This can be seen in the increasing residence times in Fig. 4.4B''. Trajectories in the neighborhood of each saddle-point stay inside for considerable durations, so the neighborhood is a metastable region (even though the saddle-point itself is invariant and unstable).

Importantly, it can be shown that such heteroclinic cycles can globally attract trajectories [154] and are also conserved under small parameter changes (they are structurally stable) [168]. Moreover, it has been shown in neural networks that heteroclinic cycles depend on the inputs to the neurons, such that the cycle is sensitive to the stimulus to the network [166]. Once the stimulus is applied, and the cycle is defined, it is robust against noise. So this mechanism can allow for robustness to noise while keeping sensitivity to inputs [166, 168]. This, on top of the cyclic behavior, means that heteroclinic cycles are important structures to perform sequential *computations* [65]. An example of this is chunking dynamics, in which a trajectory coding for a memory alternates along a heteroclinic cycle composed of further heteroclinic cycles, each corresponding to chunks of a memory [65]. As such, stable heteroclinic cycles have also been proposed as the mechanism behind experimental observations [168, 170, 167] and theoretically hypothesized as a mechanism for cognition [65, 169]. Heteroclinic cycles can be extended to heteroclinic networks; for a review, see [143].

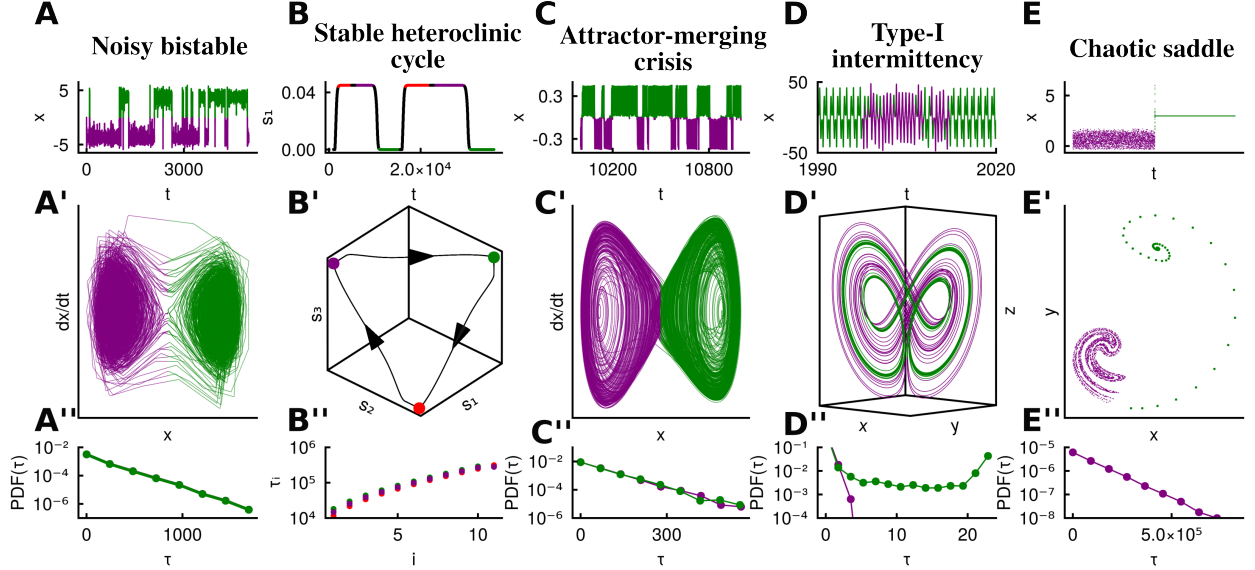


**Figure 4.4: Dynamics-based mechanisms of metastability.** Each column corresponds to a distinct mechanism. The first row (A-E) shows a representative time-series, with alternations between metastable regimes, each receiving a distinct color. The second row (A'-E') shows the state space of each system with the trajectory corresponding to the time-series above. The third row (A''-E'') shows the distribution of residence times in each metastable region for several trajectories. Further details are discussed in the main text and Supplemental Material.

Now we move to another example, which involves a *chaotic attractor* that originates from an **attractor-merging crisis** [79]. In this case, the chaotic attractor can be decomposed into two distinct sub-regions. For a different parameter value of the system, these sub-regions are separate chaotic attractors. Starting from some critical parameter value, they merge together into a combined chaotic attractor, with a specific pathway connecting them. Then, trajectories in each sub-region oscillate chaotically for a long time, on average, before they switch to the other sub-region, and repeat this process indefinitely. Figures 4.4C-C' illustrate these two intermittent regimes in a time-series and their corresponding regions in state space, respectively, colored green and purple in both. The specific pathway guiding the transitions between each sub-region is a particular periodic trajectory of type saddle (having stable and unstable manifolds) - trajectories on one sub-region approach this trajectory and then are taken to the other sub-region. It thus acts as the repelling tendency mediating the transitions between the sub-regions. The probability distribution of residence times on each of these metastable regions is exponential (Fig. 4.4C'').

It is interesting to note that the trajectories for this mechanism look similar to those for the noisy bistable systems (compare Figs. 4.4A and 4.4C). The key difference is that the transitions in the former are caused by noise, and in the latter they are caused purely by the deterministic dynamics of the system on the attractor, with the mediating saddle periodic trajectory. Still, this highlights the often apparent similarity between noisy and chaotic dynamics, and the need for deeper analysis to distinguish between both [24].

Similar dynamics occur as a result of another mechanism, an **interior crisis** [80, 156].

Also in this case, trajectories intermittently switch between two sub-regions of the same chaotic attractor. But the underlying structures are different from the attractor-merging crisis: a change of parameters causes a chaotic attractor to connect to a chaotic set that is unstable (a chaotic saddle, which we see more in Fig. 4.4E-E''). This connected chaotic attractor now includes both regions, but trajectories stay inside each sub-region for long times, before switching to the other. These transitions are again mediated by a special pathway, a periodic trajectory of saddle type, which acts as the repelling tendency. The distribution of times on the region occupied by the original chaotic attractor is again exponential. See Ref. [156] for more details.

Another example of a chaotic attractor that can be decomposed into two metastable regions occurs in **type-I intermittency**. We show in Fig. 4.4D an example in a 3-dimensional system. The trajectory alternates between metastable regimes: one with clear chaotic dynamics (in purple) and another with seemingly periodic dynamics (green). Looking at the state space in Fig. 4.4D', we note that the purple regime corresponds to a region that looks clearly chaotic (fractal-like structure), while the green regime corresponds to a region that looks like a periodic orbit (a closed loop). Trajectories can spend a considerable amount of time on the green region, looking periodic. When they leave it, they can then spend a long time in the purple region, leaving it when they approach the green region again. Mechanistically, the green region is actually the *ghost* of a stable periodic orbit that exists for different parameter values [132, 162, 192]. That stable periodic orbit is destroyed by a collision with an unstable periodic orbit at some critical parameter value, leaving behind only the ghost, which is not an invariant structure [139]. The bifurcation giving rise to this behavior is a *saddle-node bifurcation of periodic orbits*. It can also occur analogously for equilibria, and we refer the reader to Refs. [115, 194] for further work and illustrations. Importantly, the two metastable regions in our example belong to the same chaotic attractor, and the trajectories near the ghost merely *appear* to be periodic. Further, the time spent near the ghost can be considerably long, but is finite for any fixed parameter [162] (see the distribution of times in Fig. 4.4D'').

The type-I intermittency mechanism, along with the two crises discussed before, are three of many concrete instances of an idea proposed by Friston [70], who argues that different metastable regimes can correspond to different sub-regions of a same invariant set (usually attracting).

An important remark is that this mechanism does not require a chaotic attractor, as it occurs whenever a saddle-node bifurcation is nearby in parameter space. The chaotic attractor in the example only acts to re-inject the trajectories that leave the neighborhood of the ghost back onto it, creating a repeatable metastability. This re-injection can also occur due to noise, not only chaos [139]. But if there is no re-injection mechanism, nearby trajectories will pass the neighborhood of the ghost only once, and then this is an example of non-repeatable metastability.

This saddle-node mechanism has been proposed by Kelso and colleagues as a mechanism for metastability in the brain [112, 202]. Ghost structures have also been shown to play a role in the dynamics of recurrent neural networks performing particular computations [194]. Further, similarly to the idea of cycles of saddle-points (Figs. 4.4B-B''), cycles of ghost structures can also be constructed, and have been shown to generate sequences of metastable regimes that are robust in the presence of noise, having potential advantages

over cycles of saddle-points [115].

Another mechanism that leads to metastable regimes is due to a **chaotic saddle**. A chaotic saddle is similar to a chaotic attractor, with the distinction that it also has repelling directions - it is thus the analogue of a saddle equilibrium for a chaotic set [123]. As a consequence, trajectories can stay near the chaotic saddle for potentially very long times, displaying chaotic dynamics, but are eventually expelled from it [221]. Figure 4.4E shows a trajectory switching from a regime near a chaotic saddle (in purple) to one on an equilibrium (in green); the corresponding regions in state space are shown in Fig. 4.4E'. Note that the trajectories leave the chaotic saddle because they are not on it exactly; they are only near it. These are the typical trajectories, which are the ones numerically and experimentally observed. They form a metastable region even though the chaotic saddle itself is invariant and unstable. Ultimately, the trajectories converge to the stable equilibrium and remain on it infinitely long. The residence times for different initial conditions near the chaotic saddle follow an exponential distribution [80] (Fig. 4.4E'').

A chaotic saddle has been reported in networks of spiking neurons [8], in which, interestingly, it can be subdivided into three distinct dynamical regimes, corresponding to three distinct sub-regions, which are all intermittently visited for considerable durations. Therefore, also every sub-region of that chaotic saddle can be considered metastable. That is thus an example of *hierarchical metastability*, in which metastable regions contain inside more metastable regions, and the dynamics progresses through a hierarchy of metastable regimes [43]. Chaotic saddles have also been observed in other networks of spiking neurons [113, 122, 84, 108], and may play a key role in synchronization processes [140, 141].

There are several other dynamics-based mechanisms for metastability beyond the ones discussed previously. One example is **on-off intermittency**, which is common, for instance in systems that can completely synchronize [13, 157], and occurs during transitions from synchronization to desynchronization induced by changing the coupling strength between units. During these transitions, systems with on-off intermittency have trajectories that intermittently switch from a synchronized regime to a desynchronized one and back. The mechanism for this intermittency, and its statistical scaling, has been studied in detail [161, 85, 81, 223]. It is one out of many possible mechanisms that can realize the coexistence of integration (synchronization) and segregation (desynchronization), often mentioned as a crucial need for the brain [61, 202, 201, 53]. It is also a possible mechanism for the intermittent switching between UP and DOWN states exemplified in Fig. 4.1C. Furthermore, evidence for on-off intermittency has been reported for EEG data of non-convulsive paroxysmal (high-amplitude) activity in rats with genetic absence epilepsy [95]. The study identified a power-law distribution of residence times characteristic of on-off intermittency in regular brain activity, which alternated with the epileptic paroxysms. A very similar mechanism is in-out intermittency [14, 15, 183, 182]. In addition, evidence for yet another type of intermittency, known as type-III intermittency [132], has been reported in [210].

Metastability can also manifest as **mixed-mode oscillations**, in which trajectories alternate between regimes of small and large amplitude oscillations [56]. There are various mechanisms for mixed-mode oscillations, which can involve forcing the system to induce changes in parameters or through an adaptation variable that enables the switching between the two modes [56, 180]. A particular example of mixed-mode oscillations is *bursting* behavior occurring in neurons, characterized by quick firing of spikes followed by a quiescent

period (as in Fig. 4.1F). Bursting is a ubiquitous mode of firing in neurons [66], and can have important functional roles due to its ability to generate more robust responses [195]. A simple model displaying bursting is the Hindmarsh-Rose neuron [89]. In it, an adaptation current causes the switching between the tonic spiking and the silence [89]. The whole trajectory is on a stable limit cycle, but can still be decomposed into the tonic spiking and the silence, each of which can be considered metastable. This is yet another example of the idea proposed by Friston in [70]. Beyond this model, bursting behavior occurs in systems with a period-adding cascade [110]. Mixed-mode oscillations can also occur as neuronal avalanches, which are cascades of activity occurring in varying sizes and durations, and across different scales, seen in local-field potential activity [19]. An example of a dynamics-based mechanism generating avalanches has been recently elucidated in [45]. The onset of these avalanches may be associated with critical phenomena in the brain (see Ref. [77] for a recent review).

Moreover, an important example of metastable behavior is **chaotic itinerancy** [109]. This phenomenon has also been discussed in the context of neuroscience [67, 207, 208], and can include several specific mechanisms, and thus is also an umbrella term, but more specific than metastability as we define it here.

#### 4.3.4 Subtypes of metastability

The definition of metastability proposed in Sec. 4.3.2 acts as an umbrella term encompassing several distinct observations, formulations, and mechanisms. More specific formulations, which restrict the phenomenon to particular contexts, can be defined as subtypes of metastability.

As a first example, we may think of **spontaneous and driven** metastability (illustrated in Figs. 4.2G-G' respectively). They differ in regards to how transitions between metastable states are generated. In *spontaneous* metastability, the mechanism behind transition is intrinsic to the system, and thus occurs without the need of external perturbations - such as noise, or stimuli. This is the case for Figs. 4.4B-E''. Driven metastability is the opposite: transitions occur because of external perturbations, as in Fig. 4.4A-A''. Each subtype has distinct but important functional roles: spontaneous metastability enables transitions between regimes without the expenditure of additional energy to stimulate the transitions [202], and guarantees that a system does not get stuck in the same regime [102]; driven metastability is important for direct control of the transitions, such as in stimulus-evoked scenarios.

A second important pair of subtypes is **repeatable versus non-repeatable metastability** (Figs. 4.2H-H'). These are characterized by whether the metastable regimes eventually repeat in the time series or not. If the metastable regimes repeat along observations, the metastability is repeatable; if they do not, it is non-repeatable. The case of non-repeatable regimes is sometimes called metastability en route to ground state [28]. Note that the observations in Fig. 4.1 and the mechanisms in Fig. 4.4 are already classified into these subtypes.

## 4.4 Conclusions and outlook

In this Perspective we have provided a discussion on metastable brain dynamics in a way that is consistent across observations and theory in both neuroscience and dynamical systems. With this, we have looked into several dynamics-based mechanisms that generate metastability, and compared them to obtain insights into their commonalities, distinctions, and connections to previous literature.

The first step was to extract a general definition of metastability from the literature: metastable regimes are long-lived but transient. This serves as an umbrella term encompassing the other formulations in the literature, is useful to interpret observations, and readily connects to dynamical systems theory. We then looked deeper into how these metastable regimes behave in state space. To achieve this, we introduced the notion of almost-invariant regions of state space, characterized by a high probability (smaller than one) that trajectories, once inside them, remain inside [71, 55]. Trajectories can enter an almost-invariant region, stay inside for a long time, and eventually leave. While inside such a region, trajectories exhibit time-series containing long-lived but transient epochs with unique dynamical properties, i.e. metastable regimes. The dynamics of the regimes corresponds to the dynamics in the regions (e.g., periodic or chaotic). Thus, almost-invariant regions, which we identify as metastable regions, underlie the dynamics of metastable regimes.

With this view, we have then discussed the *dynamics-based mechanisms* for metastability, i.e. how metastable regions and regimes are generated, and how they behave. Dynamical systems theory provides several concrete possibilities. Some of these have been previously discussed in the neuroscientific context [78, 43, 28], but some are also new, to the best of our knowledge. Though not a comprehensive list, we believe it serves as a good starting point for researchers both in neuroscience and dynamical systems intending to study metastability.

Looking at so many different mechanisms together provides several insights. To start, it provides concrete examples of metastable regimes corresponding to trajectories visiting metastable (almost-invariant) regions. Further, it becomes clear that around each metastable region there is a *coexistence of attracting and repelling tendencies in state space*, as has been discussed in Refs. [202, 109]. These realizations further validate the definition, which is general but still meaningful to allow for common underlying principles.

With this rich list of possible mechanisms, we have been able to provide several concrete instances of an idea that was abstractly proposed by Friston in Ref. [70]: that the same attractor can have multiple sub-regions, each corresponding to one metastable regime. An interesting instance of this has been reported in Ref. [8], in which networks of spiking neurons display a chaotic saddle (its neighborhood a metastable region) that can be further subdivided into three sub-regions, each metastable and corresponding to different patterns of activity.

We have also suggested more dynamics-based mechanisms that can account for the important behavior of coexistence of segregation and integration: besides the important saddle-node bifurcation of fixed points that often occurs [202], we also mention in-out and on-off intermittency as mechanisms that lead to variability of synchronization [13, 183].

The solid theoretical background offered by the idea of almost-invariant regions allows us to provide objective answers to issues debated in the literature. The distinction between at-

tractors and metastable regions, and hence between *multistability* and *metastability* becomes clear. As discussed in Sections 4.3.1 and 4.3.2, attractors are invariant: trajectories on them remain on them infinitely long; meanwhile, metastable regions are only almost-invariant: trajectories eventually leave them. A system is called multistable when it has multiple co-existing attractors for fixed parameters, a typical behavior in nonlinear dynamical systems [59, 60]. In a multistable system, trajectories converge to one of the attractors, selected by their initial conditions, and remain on this attractor forever. There are no transitions between attractors in a multistable system. If external perturbations such as noise are introduced to a multistable system, the trajectories do not stick to attractors anymore, but can hop between them [100]. In this case, multistability is *substituted* by metastability [160]. An important remark is that, when the noise is too strong, it can overpower any dynamics of the system and then there is neither multistability nor metastability observable, only a random motion [116]. Crucially, however, stability (and multistability) can *co-occur* with metastability in autonomous systems, without noise. For instance, an attractor can be in some cases decomposed into two or more metastable regions, as discussed previously and in Sec. 4.3.3. Then, trajectories remain eternally inside an attractor, but with transitions between its metastable regions.

Another point that is often debated is whether both *spontaneous* and *noise-induced* cases should be considered as metastable [111, 43, 96]. Here, we provide an objective answer: since there are almost-invariant regions underlying the dynamics in both cases, both are metastable. This is exemplified through the motion in the double-well landscape with noise (Figs. 4.4A-A'') and the intermittency due to an attractor-merging crisis (Figs. 4.4C-C''), in which also the phenomenology in the time-series, in state space, and in the distribution of residence times is strikingly similar. This means that many dynamics-based mechanisms may underlie the same observation. Therefore, the characterization of regimes as metastable is only part of the story: they possess other dynamical properties that also need to be studied. Developing methods to achieve this and properly distinguish between various mechanisms is still a subject of future research.

Understanding dynamics-based mechanisms is an important first step for *predicting* transitions between metastable regimes. This is particularly important in the context of seizure prediction, an area that has deservedly received a lot of attention but which still has many open questions [119]. Knowledge of the dynamics-based mechanism underlying transitions from normal brain activity to seizures has been recognized as a key development in the field [119], but that alone may not be enough: part of the difficulty may be the co-existence of several mechanisms, not just one. A more comprehensive understanding of the mechanisms for metastability, extending the ideas proposed here, could prove useful to address these difficulties through a better understanding of the precursor dynamics of transitions [173]. A possible future path can also aim to determine mechanisms underlying observations through the use of techniques to identify system equations from data [213, 29, 196, 9, 103].

Finally, we believe it is worth mentioning that transient or metastable dynamics have been recognized as important mechanisms for *computations* in the brain [65, 39, 215, 124, 136, 194] and other biological systems [150, 149]. Research has shown that systems can successfully perform computations with attractors [114] or with transient regimes [136, 35, 124, 114, 20, 32, 129]. This, allied with the observations of complex metastable dynamics in the brain [28], brings up the question: what advantages can spontaneous metastable regimes provide

for computations, in contrast to stable regimes? This is a crucial question that needs to be addressed in future works, and may use the ideas proposed here as a starting point.

Therefore, we believe that the perspective we provide here connects observations, formulations, and mechanisms of metastability in neuroscience with the goal of understanding metastable brain dynamics.

## Acknowledgments

We would like to thank Klaus Lehnertz, James A. Yorke, Niccolò Zagli, Nicolás Rubido, and Péter Koltai for inspiring discussions. In particular we would like to deeply thank Klaus Lehnertz for comments on this manuscript. K.L.R. was supported by the German Academic Exchange Service (DAAD). E.S.M and U.F. acknowledge the support by the Deutsche Forschungsgemeinschaft (DFG) via the project number 454054251. B.R.R.B. acknowledges the support of the São Paulo Research Foundation (FAPESP), Brazil, Proc. 2018/03211-6 and 2021/09839-0. This work was partially supported by BrainsCAN at Western University through the Canada First Research Excellence Fund (CFREF), the NSF through a NeuroNex award (#2015276), the Natural Sciences and Engineering Research Council of Canada (NSERC) grant R0370A01, and the Western Academy for Advanced Research. R.C.B gratefully acknowledges the Western Institute for Neuroscience Clinical Research Postdoctoral Fellowship.

## Supplementary material

### 4.4.1 Models

The code used to generate Figure 4 in the main text is available in the GitHub repository [178]. The data used can be made available upon request. All the code is done in the Julia computational language [21]; integration was done with the package DifferentialEquations.jl [171], with the aid of packages DynamicalSystems.jl [49] and DrWatson.jl [50]. Plots were made with Makie.jl [48].

#### Noisy bistable system

The noisy bistable system, also known as the noisy Duffing oscillator [192], is given by:

$$dx = v + \eta_1 dW \tag{4.1}$$

$$dv = -ax^3 + bx - c - dv + \eta_2 dW, \tag{4.2}$$

with  $dW$  describing a white Gaussian noise. The equations describe the evolution of a particle on a double-well (quartic) potential  $U(x) = ax^4/4 - bx^2/2 + cx$  being periodically driven and with noise. The parameters used were  $a = 0.5$ ;  $b = 8.0$ ,  $c = 0.0$ ,  $d = 0.2$ ,  $\eta_1 = \eta_2 = 0.18$ , with initial condition  $(0, 0)$ .

## The heteroclinic cycle

The heteroclinic cycle occurs in a rate model derived from Hodgkin-Huxley type neurons with synaptic coupling [16]. The equations are given by:

$$\tau \dot{s}_i = (r_i - s_i/2) \frac{S_{\max} - s_i}{S_{\max}} \quad (4.3)$$

$$\tau \dot{r}_i = x_0 F \left( I - \sum_{j=1}^N g_{ij} s_j \right) \tau - r_i \quad (4.4)$$

for  $i = 1, 2, 3$ , with

$$F(x) = \exp(-\epsilon/x) [\max(0, x)^\alpha]. \quad (4.5)$$

The matrix  $g$  is constructed such that  $g_{21} = g_{32} = g_{13} = g_1$ ,  $g_{12} = g_{23} = g_{31} = g_2$  and  $g_{11} = g_{22} = g_{33} = 0$ . The parameters are  $\tau = 50$ ,  $\epsilon = 10^{-3}$ ,  $I = 0.145$ ,  $S_{\max} = 0.045$ ,  $g_1 = 3.0$ ,  $g_2 = 0.7$ ,  $x_0 = 2.57 \times 10^{-3}$ , and  $\alpha = 0.564$ .

The numerical integration is best done with a change of coordinates  $z_i \equiv \log(S_{\max} - s_i)$ , which reduces the numerical precision difficulties associated with the trajectory getting too close to the stable manifold of the fixed points. The initial condition was  $(0.5, 0.2, 0.4, 0.9, 0.5, 0.6)$ .

## Attractor-merging crisis

We have provided an example of attractor-merging crisis for the Duffing oscillator, whose dynamics is described by [101]:

$$\dot{x} = v \quad (4.6)$$

$$\dot{v} = -ax^3 + bx - dv + f \cos(\omega t), \quad (4.7)$$

with parameters  $a = 100$ ,  $b = 10$ ,  $d = 1.0$ ,  $f = 0.852$ ,  $\omega = 3.5$  and initial condition  $(x, v) = (0.11, 0.11)$ .

## Type-I intermittency

The system used to obtain the type I intermittency is the Lorenz63 model [130]. The equations are given by

$$\dot{x} = \sigma(y - x) \quad (4.8)$$

$$\dot{y} = x(\rho - z) - y \quad (4.9)$$

$$\dot{z} = xz - \beta z. \quad (4.10)$$

The parameters used in the figure are  $\sigma = 10$ ,  $\beta = 8/3$  and  $\rho = 166.1$ , based on [221]. The parameter used to obtain a stable limit cycle (before the saddle-node bifurcation) was  $\rho = 166.06$ . The initial condition was  $(0.1, 0.1, 0.1)$ .

## Chaotic saddle

The chaotic saddle shown in the Fig. 4E-E'' occurs in the Ikeda system [7], which has discretized time:

$$x_{n+1} = a + b(x_n \cos(t_n) - y_n \sin(t_n)) \quad (4.11)$$

$$y_{n+1} = b(x_n \sin(t_n) + y_n \cos(t_n)), \quad (4.12)$$

with

$$t_n = c - \frac{d}{1 + x_n^2 + y_n^2}. \quad (4.13)$$

The parameters used for the chaotic saddle were  $b = 0.9$ ,  $c = 0.4$ ,  $d = 6.0$ ,  $a = 1.003$ . The saddle exists due to a boundary crisis, which occurs for a slightly smaller  $a$ . For reference, the value of  $a$  used to obtain a chaotic attractor was  $a = 0.997$ . The initial condition was  $(2.97, 4.15)$ . This is the only mechanism in the figure where the initial condition is important: to reproduce the behavior, the trajectories need to be initialized near the chaotic saddle.

### 4.4.2 Brief notion of almost-invariant sets

Following Ref. [71], we provide a brief notion of almost-invariant sets for a mapping  $T : X \rightarrow X$ , with  $X$  being the state space, but it can also be formulated for flows [74]. To formalize the notion of almost-invariant sets, we need to first define a natural measure on any set  $A$ . This corresponds to the fraction of time that typical trajectories, starting in  $x \in X$ , spend on that set along their evolution:

$$\mu(A) = \lim_{N \rightarrow \infty} \frac{\#\{i \in [0, N-1] : T^i x \in A\}}{N} \quad (4.14)$$

The probability of trajectories, once inside  $A$ , to remain in  $A$ , is computed as

$$\rho(A) = \text{Prob}(Tx \in A | x \in A) = \frac{\mu(T^{-1}A \cap A)}{\mu(A)}. \quad (4.15)$$

A set  $A$  is then said to be almost-invariant if  $\rho(A)$  is high but not 1, meaning that trajectories, once inside  $R$ , have a high probability of remaining in  $R$ . Suppose that the state space can be divided into disjointed almost-invariant sets  $\{R_1, R_2, \dots, R_N\}$ . One can obtain maximally almost-invariant sets by maximizing the mean probability  $\frac{1}{N} \sum_{i=1}^N \rho(A_i)$  [71, 72].

# Appendix A

## Code listing

```
1 function print_rate(kappa,xMin,xMax,npoints,option)
2     local c = 1-kappa*kappa
3     local croot = (1-kappa*kappa)^(1/2)
4     local logx = math.log(xMin)
5     local psi = 0
6
7     local xstep = (math.log(xMax)-math.log(xMin))/(npoints-1)
8
9     arg0 = math.sqrt(xMin/c)
10    psi0 = (1/c)*math.exp((kappa*arg0)^2)*(erfc(kappa*arg0)-erfc(
11        arg0))
12
13    if option==[] then
14        tex.sprint("\addplot+["..option.." ] coordinates{")
15        -- addplot+ for color cycle to work
16    else
17        tex.sprint("\addplot+ coordinates{")
18    end
19    tex.sprint("("..xMin.." , "..psi0.." )")
20
21    for i=1, (npoints-1) do
22        x = math.exp(logx + xstep)
23        arg = math.sqrt(x/c)
24        karg = kappa*arg
25        if karg<5 then
26            -- this break compensates for exp(karg^2), which multiplies the
27            -- error in the erf approximation...
28            logpsi = -math.log(croot) + karg^2 + math.log(erfc(karg)-
29                erfc(arg))
30            psi = math.exp(logpsi)
31        else
32            psi = (1/(karg) - 1/(2*(karg^3)) + 3/(4*(arg^5))) / (1
33                .77245385*croot)
```

```
30      -- this is the large x asymptote of the reaction rate
31  end
32  logx = math.log(x)
33  tex.sprint("("..x.." , "..psi..")")
34  end
35  tex.sprint("}")
36 end
37 \end{luacode*}
```

# Bibliography

- [1] M Abeles, H Bergman, I Gat, I Meilijson, E Seidemann, N Tishby, and E Vaadia. Cortical activity flips among quasi-stationary states. *Proceedings of the National Academy of Sciences*, 92(19):8616–8620, 1995.
- [2] Juan A. Acebrón, L. L. Bonilla, Conrad J. Pérez Vicente, Félix Ritort, and Renato Spigler. The Kuramoto model: A simple paradigm for synchronization phenomena. *Reviews of Modern Physics*, 77(1):137–185, 2005.
- [3] Valentin S. Afraimovich, Mehmet K. Muezzinoglu, and Mikhail I. Rabinovich. Long-range Interactions, Stochasticity and Fractional Dynamics, Dedicated to George M. Zaslavsky (1935–2008). *Nonlinear Physical Science*, pages 133–175, 2010.
- [4] Miguel Aguilera, Manuel G. Bedia, and Xabier E. Barandiaran. Extended neural metastability in an embodied model of sensorimotor coupling. *Frontiers in Systems Neuroscience*, 10(SEP):76, 2016.
- [5] Réka Albert and Albert-László Barabási. Statistical mechanics of complex networks. *Reviews of Modern Physics*, 74(1):47–97, 2002.
- [6] Thomas H. Alderson, Arun L. W. Bokde, J. A. Scott Kelso, Liam Maguire, and Damien Coyle. Metastable neural dynamics underlies cognitive performance across multiple behavioural paradigms. *Human Brain Mapping*, 41(12):3212–3234, 2020.
- [7] Kathleen T. Alligood, Tim D. Sauer, and James A. Yorke. *Chaos: An Introduction to Dynamical Systems*. Textbooks in Mathematical Sciences. Springer Berlin Heidelberg, Berlin, Heidelberg, 1996.
- [8] Gerrit Ansmann, Klaus Lehnertz, and Ulrike Feudel. Self-induced switchings between multiple space-time patterns on complex networks of excitable units. *Physical Review X*, 6(1):011030, 2016.
- [9] Mehrnaz Anvari, M. Reza Rahimi Tabar, Joachim Peinke, and Klaus Lehnertz. Disentangling the stochastic behavior of complex time series. *Scientific Reports*, 6(1):35435, 2016.
- [10] F. T. Arecchi, R. Badii, and A. Politi. Generalized multistability and noise-induced jumps in a nonlinear dynamical system. *Physical Review A*, 32(1):402–408, 1985.

- [11] Alex Arenas, Albert Díaz-Guilera, Jurgen Kurths, Yamir Moreno, and Changsong Zhou. Synchronization in complex networks. *Physics Reports*, 469(3):93–153, 2008.
- [12] Lluís Arola-Fernández, Sergio Faci-Lázaro, Per Sebastian Skardal, Emanuel-Cristian Boghiu, Jesús Gómez-Gardeñes, and Alex Arenas. Emergence of explosive synchronization bombs in networks of oscillators. *Communications Physics*, 5(1):264, 2022.
- [13] Peter Ashwin, Jorge Buescu, and Ian Stewart. Bubbling of attractors and synchronisation of chaotic oscillators. *Physics Letters A*, 193(2):126–139, 1994.
- [14] Peter Ashwin, Eurico Covas, and Reza Tavakol. Transverse instability for non-normal parameters. *Nonlinearity*, 12(3):563–577, 1999.
- [15] Peter Ashwin, Eurico Covas, and Reza Tavakol. Influence of noise on scalings for in-out intermittency. *Physical Review E*, 64(6):066204, 2001.
- [16] Peter Ashwin, Ozkan Karabacak, and Thomas Nowotny. Criteria for robustness of heteroclinic cycles in neural microcircuits. *The Journal of Mathematical Neuroscience*, 1(1):13, 2011.
- [17] Peter Ashwin and Marc Timme. When instability makes sense. *Nature*, 436(7047):36–37, 2005.
- [18] A Babloyantz and A Destexhe. Low-dimensional chaos in an instance of epilepsy. *Proceedings of the National Academy of Sciences*, 83(10):3513–3517, 1986.
- [19] John M Beggs and Dietmar Plenz. Neuronal avalanches in neocortical circuits. *Journal of neuroscience*, 23(35):11167–11177, 2003.
- [20] Gabriel B. Benigno, Roberto C. Budzinski, Zachary W. Davis, John H. Reynolds, and Lyle Muller. Waves traveling over a map of visual space can ignite short-term predictions of sensory input. *Nature Communications*, 14(1):3409, 2023.
- [21] Jeff Bezanson, Alan Edelman, Stefan Karpinski, and Viral B Shah. Julia: A fresh approach to numerical computing. *SIAM Review*, 59(1):65–98, 2017.
- [22] David Bhowmik and Murray Shanahan. Metastability and Inter-Band Frequency Modulation in Networks of Oscillating Spiking Neuron Populations. *PLoS ONE*, 8(4):e62234, 2013.
- [23] K. Binder. Finite size effects on phase transitions. *Ferroelectrics*, 73(1):43–67, 1987.
- [24] B. R. R. Boaretto, R. C. Budzinski, K. L. Rossi, T. L. Prado, S. R. Lopes, and C. Masoller. Discriminating chaotic and stochastic time series using permutation entropy and artificial neural networks. *Scientific Reports*, 11(1):15789, 2021.
- [25] Jordan G Brankov, Daniel M Danchev, and Nicholai S Tonchev. *Theory of Critical Phenomena in Finite-Size Systems*. World Scientific, 2000.

- [26] Markus Brede. Synchrony-optimized networks of non-identical Kuramoto oscillators. *Physics Letters, Section A: General, Atomic and Solid State Physics*, 372(15):2618–2622, 2008.
- [27] Steven L Bressler and J A Scott Kelso. Coordination dynamics in cognitive neuroscience. *Frontiers in Neuroscience*, 10:397, 2016.
- [28] B. A. W. Brinkman, H. Yan, A. Maffei, I. M. Park, A. Fontanini, J. Wang, and G. La Camera. Metastable dynamics of neural circuits and networks. *Applied Physics Reviews*, 9(1):011313, 2022.
- [29] Steven L. Brunton, Joshua L. Proctor, and J. Nathan Kutz. Discovering governing equations from data by sparse identification of nonlinear dynamical systems. *Proceedings of the National Academy of Sciences*, 113(15):3932–3937, 2016.
- [30] R. C. Budzinski, B. R. R. Boaretto, T. L. Prado, R. L. Viana, and S. R. Lopes. Synchronous patterns and intermittency in a network induced by the rewiring of connections and coupling. *Chaos: An Interdisciplinary Journal of Nonlinear Science*, 29(12):123132, 2019.
- [31] R. C. Budzinski, K. L. Rossi, B. R. R. Boaretto, T. L. Prado, and S. R. Lopes. Synchronization malleability in neural networks under a distance-dependent coupling. *Physical Review Research*, 2(4):043309, 2020.
- [32] Roberto C Budzinski, Alexandra N Busch, Samuel Mestern, Erwan Martin, Luisa H B Liboni, Federico W Pasini, Ján Mináč, Todd Coleman, Wataru Inoue, and Lyle E Muller. An exact mathematical description of computation with transient spatiotemporal dynamics in a complex-valued neural network. *arXiv*, 2023.
- [33] Roberto C. Budzinski, Tung T. Nguyen, Jacqueline Doàn, Ján Mináč, Terrence J. Sejnowski, and Lyle E. Muller. Geometry unites synchrony, chimeras, and waves in nonlinear oscillator networks. *Chaos*, 32(3):031104, 2022.
- [34] Victor Buenda, Pablo Villegas, Raffaella Burioni, and Miguel A. Muoz. The broad edge of synchronization: Griffiths effects and collective phenomena in brain networks. *Philosophical Transactions of the Royal Society A*, 380(2227):20200424, 2022.
- [35] Dean V. Buonomano and Wolfgang Maass. State-dependent computations: spatiotemporal processing in cortical networks. *Nature Reviews Neuroscience*, 10(2):113–125, 2009.
- [36] Lubos Buzna, Sergi Lozano, and Albert Díaz-Guilera. Synchronization in symmetric bipolar population networks. *Physical Review E*, 80(6):066120, 2009.
- [37] Joana Cabral, Etienne Hugues, Olaf Sporns, and Gustavo Deco. Role of local network oscillations in resting-state functional connectivity. *Neuroimage*, 57(1):130–139, 2011.
- [38] Herbert B. Callen. *Thermodynamics and an Introduction to Thermostatistics*. Wiley, 2 edition, 1991.

- [39] Giancarlo La Camera, Alfredo Fontanini, and Luca Mazzucato. Cortical computations via metastable activity. *Current Opinion in Neurobiology*, 58:37–45, 2019.
- [40] R. Carareto, F. M. Orsatti, and J. R.C. Piqueira. Optimized network structure for full-synchronization. *Communications in Nonlinear Science and Numerical Simulation*, 14(6):2536–2541, 2009.
- [41] Nicole Carlson, Dong-Hee Kim, and Adilson E. Motter. Sample-to-sample fluctuations in real-network ensembles. *Chaos: An Interdisciplinary Journal of Nonlinear Science*, 21(2):025105, 2011.
- [42] Valeria C. Caruso, Jeff T. Mohl, Christopher Glynn, Jungah Lee, Shawn M. Willett, Azeem Zaman, Akinori F. Ebihara, Rolando Estrada, Winrich A. Freiwald, Surya T. Tokdar, and Jennifer M. Groh. Single neurons may encode simultaneous stimuli by switching between activity patterns. *Nature Communications*, 9(1):2715, 2018.
- [43] Federico Cavanna, Martina G. Vilas, Matías Palmucci, and Enzo Tagliazucchi. Dynamic functional connectivity and brain metastability during altered states of consciousness. *NeuroImage*, 180(Pt B):383–395, 2018.
- [44] Diego Contreras, Alain Destexhe, Terrence J. Sejnowski, and Mircea Steriade. Control of Spatiotemporal Coherence of a Thalamic Oscillation by Corticothalamic Feedback. *Science*, 274(5288):771–774, 1996.
- [45] Max Contreras, Everton S. Medeiros, Anna Zakharova, Philipp Hövel, and Igor Franović. Scale-free avalanches in arrays of FitzHugh–Nagumo oscillators. *Chaos: An Interdisciplinary Journal of Nonlinear Science*, 33(9):093106, 2023.
- [46] Patrick Crotty, Dan Schult, and Ken Segall. Josephson junction simulation of neurons. *Physical Review E*, 82(1):011914, 2010.
- [47] Marco de Curtis and Massimo Avoli. Initiation, Propagation, and Termination of Partial (Focal) Seizures. *Cold Spring Harbor Perspectives in Medicine*, 5(7):a022368, 2015.
- [48] Simon Danisch and Julius Krumbiegel. Makie.jl: Flexible high-performance data visualization for Julia. *Journal of Open Source Software*, 6(65):3349, 2021.
- [49] George Datseris. DynamicalSystems.jl: A Julia software library for chaos and nonlinear dynamics. *Journal of Open Source Software*, 3(23):598, 2018. Publisher: The Open Journal.
- [50] George Datseris, Jonas Isensee, Sebastian Pech, and Tamás Gál. DrWatson: the perfect sidekick for your scientific inquiries. *Journal of Open Source Software*, 5(54):2673, 2020.
- [51] Gustavo Deco and Morten L. Kringelbach. Metastability and Coherence: Extending the Communication through Coherence Hypothesis Using A Whole-Brain Computational Perspective. *Trends in Neurosciences*, 39(3):125–135, 2016.

- [52] Gustavo Deco, Morten L. Kringelbach, Viktor K. Jirsa, and Petra Ritter. The dynamics of resting fluctuations in the brain: Metastability and its dynamical cortical core. *Scientific Reports*, 7(1):3095, 2017.
- [53] Gustavo Deco, Giulio Tononi, Melanie Boly, and Morten L. Kringelbach. Rethinking segregation and integration: contributions of whole-brain modelling. *Nature Reviews Neuroscience*, 16(7):430–439, 2015.
- [54] Stanislas Dehaene and Jean-Pierre Changeux. Ongoing Spontaneous Activity Controls Access to Consciousness: A Neuronal Model for Inattentional Blindness. *PLoS Biology*, 3(5):e141, 2005.
- [55] Michael Dellnitz and Robert Preis. Symbolic and Numerical Scientific Computation, Second International Conference, SNSC 2001, Hagenberg, Austria, September 12–14, 2001. Revised Papers. *Lecture Notes in Computer Science*, pages 183–209, 2003.
- [56] Mathieu Desroches, John Guckenheimer, Bernd Krauskopf, Christian Kuehn, Hinke M. Osinga, and Martin Wechselberger. Mixed-Mode Oscillations with Multiple Time Scales. *SIAM Review*, 54(2):211–288, 2012.
- [57] Jennifer A. Dunne, Richard J. Williams, and Neo D. Martinez. Food-web structure and network theory: The role of connectance and size. *Proceedings of the National Academy of Sciences*, 99(20):12917–12922, 2002.
- [58] Laura M. J. Fernandez and Anita Lüthi. Sleep Spindles: Mechanisms and Functions. *Physiological Reviews*, 100(2):805–868, 2020.
- [59] Ulrike Feudel. Complex Dynamics In Multistable Systems. *International Journal of Bifurcation and Chaos*, 18(06):1607–1626, 2008.
- [60] Ulrike Feudel, Alexander N. Pisarchik, and Kenneth Showalter. Multistability and tipping: From mathematics and physics to climate and brain - Minireview and preface to the focus issue. *Chaos*, 28(3):33501, 2018.
- [61] Andrew A. Fingelkurts and Alexander A. Fingelkurts. Operational architectonics of the human brain biopotential field: Towards solving the mind-brain problem. *Brain and Mind*, 2(3):261–296, 2001. ISSN: 13891987 Publication Title: Brain and Mind.
- [62] Andrew A Fingelkurts and Alexander A Fingelkurts. Timing in cognition and EEG brain dynamics: discreteness versus continuity. *Cognitive Processing*, 7(3):135–162, 2006.
- [63] Andrew A Fingelkurts and Alexander A Fingelkurts. Brain-Mind Operational Architectonics Imaging: Technical and Methodological Aspects. *The Open Neuroimaging Journal*, 2:73–93, 2008.
- [64] Andrew A. Fingelkurts and Alexander A. Fingelkurts. Information flow in the brain: Ordered sequences of metastable states. *Information (Switzerland)*, 8(1):1–9, 2017.

- [65] Jordi Fonollosa, Emre Neftci, and Mikhail Rabinovich. Learning of Chunking Sequences in Cognition and Behavior. *PLOS Computational Biology*, 11(11):e1004592, 2015.
- [66] David M Fox, Horacio G Rotstein, and Farzan Nadim. Bursting in neurons and small networks. In Dieter Jaeger and Ranu Jung, editors, *Encyclopedia of computational neuroscience*, pages 455–469. Springer New York, New York, NY, 2015.
- [67] Freeman and J. Walter. Evidence from human scalp electroencephalograms of global chaotic itinerancy. *Chaos: An Interdisciplinary Journal of Nonlinear Science*, 13(3):1067–1077, 2003.
- [68] Pascal Fries. Rhythms for Cognition: Communication through Coherence. *Neuron*, 88(1):220–235, 2015.
- [69] Friston and J. Karl. Transients, metastability, and neuronal dynamics. *NeuroImage*, 5(2):164–171, 1997.
- [70] K J Friston. The labile brain. II. Transients, complexity and selection. *Philosophical Transactions of the Royal Society of London. Series B, Biological Sciences*, 355(1394):237–252, 2000.
- [71] Gary Froyland. Statistically optimal almost-invariant sets. *Physica D: Nonlinear Phenomena*, 200(3-4):205–219, 2005.
- [72] Gary Froyland and Michael Dellnitz. Detecting and Locating Near-Optimal Almost-Invariant Sets and Cycles. *SIAM Journal on Scientific Computing*, 24(6):1839–1863, 2003.
- [73] Gary Froyland and Oliver Junge. Robust FEM-Based Extraction of Finite-Time Coherent Sets Using Scattered, Sparse, and Incomplete Trajectories. *SIAM Journal on Applied Dynamical Systems*, 17(2):1891–1924, 2018.
- [74] Gary Froyland and Kathrin Padberg. Almost-invariant sets and invariant manifolds — Connecting probabilistic and geometric descriptions of coherent structures in flows. *Physica D: Nonlinear Phenomena*, 238(16):1507–1523, 2009.
- [75] Maximilian Gelbrecht, Jürgen Kurths, and Frank Hellmann. Monte Carlo basin bifurcation analysis. *New Journal of Physics*, 22(3):033032, 2020.
- [76] Tommaso Gili, Valentina Ciullo, and Gianfranco Spalletta. Metastable States of Multiscale Brain Networks Are Keys to Crack the Timing Problem. *Frontiers in Computational Neuroscience*, 12:75, 2018.
- [77] Mauricio Girardi-Schappo. Brain criticality beyond avalanches: open problems and how to approach them. *Journal of Physics: Complexity*, 2(3):031003, 2021.
- [78] Peter beim Graben, Antonio Jimenez-Marin, Ibai Diez, Jesus M. Cortes, Mathieu Desroches, and Serafim Rodrigues. Metastable Resting State Brain Dynamics. *Frontiers in Computational Neuroscience*, 13:62, 2019.

- [79] Celso Grebogi, Edward Ott, Filipe Romeiras, and James A. Yorke. Critical exponents for crisis-induced intermittency. *Physical Review A*, 36(11):5365–5380, 1987.
- [80] Celso Grebogi, Edward Ott, and James A. Yorke. Crises, sudden changes in chaotic attractors, and transient chaos. *Physica D: Nonlinear Phenomena*, 7(1-3):181–200, 1983.
- [81] P W Hammer, N Platt, S M Hammel, J F Heagy, and B D Lee. Experimental observation of on-off intermittency. *Physical Review Letters*, 73(8):1095–1098, 1994.
- [82] Edward J. Hancock and Georg A. Gottwald. Model reduction for Kuramoto models with complex topologies. *Physical Review E*, 98(1):012307, 2018.
- [83] Peter Hanggi. Escape from a metastable state. *Journal of Statistical Physics*, 42(1-2):105–148, 1986.
- [84] Harrison Hartle and Renate Wackerbauer. Transient chaos and associated system-intrinsic switching of spacetime patterns in two synaptically coupled layers of Morris-Lecar neurons. *Physical Review E*, 96(3):032223, 2017.
- [85] J. F. Heagy, N. Platt, and S. M. Hammel. Characterization of on-off intermittency. *Physical Review E*, 49(2):1140–1150, 1994.
- [86] Peter J. Hellyer, Gregory Scott, Murray Shanahan, David J. Sharp, and Robert Leech. Cognitive Flexibility through Metastable Neural Dynamics Is Disrupted by Damage to the Structural Connectome. *The Journal of Neuroscience*, 35(24):9050–9063, 2015.
- [87] Peter J. Hellyer, Murray Shanahan, Gregory Scott, Richard J.S. Wise, David J. Sharp, and Robert Leech. The control of global brain dynamics: Opposing actions of frontoparietal control and default mode networks on attention. *Journal of Neuroscience*, 34(2):451–461, 2014.
- [88] Eric J. Hildebrand, Michael A. Buice, and Carson C. Chow. Kinetic Theory of Coupled Oscillators. *Physical Review Letters*, 98(5):054101, 2007.
- [89] J. L. Hindmarsh and R. M. Rose. A model of neuronal bursting using three coupled first order differential equations. *Proceedings of the Royal Society of London. Series B. Biological Sciences*, 221(1222):87–102, 1984.
- [90] H. Hong, M. Y. Choi, and Beom Jun Kim. Synchronization on small-world networks. *Physical Review E*, 65(2):1–5, 2002.
- [91] Hyunsuk Hong, Hugues Chaté, Hyunggyu Park, and Lei Han Tang. Entrainment transition in populations of random frequency oscillators. *Physical Review Letters*, 99(18):1–4, 2007.
- [92] Hyunsuk Hong, Hyunggyu Park, and Lei-Han Tang. Anomalous Binder Cumulant and Lack of Self-Averageness in Systems with Quenched Disorder. *Journal of the Korean Physical Society*, 49(5):L1885–L1889, 2006.

- [93] Hyunsuk Hong, Hyunggyu Park, and Lei Han Tang. Finite-size scaling of synchronized oscillation on complex networks. *Physical Review E*, 76(6):1–7, 2007.
- [94] Hyunsuk Hong, Jaegon Um, and Hyunggyu Park. Link-disorder fluctuation effects on synchronization in random networks. *Physical Review E - Statistical, Nonlinear, and Soft Matter Physics*, 87(4):1–5, 2013.
- [95] Alexander Hramov, Alexey A. Koronovskii, I. S. Midzyanovskaya, E. Sitnikova, and C. M. van Rijn. On-off intermittency in time series of spontaneous paroxysmal activity in rats with genetic absence epilepsy. *Chaos: An Interdisciplinary Journal of Nonlinear Science*, 16(4):043111, 2006.
- [96] Hudson and E. Andrew. Metastability of neuronal dynamics during general anesthesia: Time for a change in our assumptions? *Frontiers in Neural Circuits*, 11:58, 2017.
- [97] Andrew E Hudson, Diany Paola Calderon, Donald W Pfaff, and Alex Proekt. Recovery of consciousness is mediated by a network of discrete metastable activity states. *Proceedings of the National Academy of Sciences of the United States of America*, 111(25):9283–9288, 2014.
- [98] Mark D. Humphries and Kevin Gurney. Network ‘Small-World-Ness’: A Quantitative Method for Determining Canonical Network Equivalence. *PLoS ONE*, 3(4):e2051, 2008.
- [99] John D Hunter. Matplotlib: A 2D Graphics Environment. *Computing in science & engineering*, 9(3):90–95, 2007.
- [100] Peter Hänggi, Peter Talkner, and Michal Borkovec. Reaction-rate theory: fifty years after Kramers. *Reviews of Modern Physics*, 62(2):251–341, 1990.
- [101] Hiroaki Ishii, Hirokazu Fujisaka, and Masayoshi Inoue. Breakdown of chaos symmetry and intermittency in the double-well potential system. *Physics Letters A*, 116(6):257–263, 1986.
- [102] Junji Ito, Andrey R. Nikolaev, and Cees van Leeuwen. Dynamics of spontaneous transitions between global brain states. *Human Brain Mapping*, 28(9):904–913, 2007.
- [103] Mozes Jacobs, Bingni W Brunton, Steven L Brunton, J Nathan Kutz, and Ryan V Raut. HyperSINDy: Deep Generative Modeling of Nonlinear Stochastic Governing Equations. *arXiv*, 2023.
- [104] Daniel Jercog, Alex Roxin, Peter Barthó, Artur Luczak, Albert Compte, and Jaime de la Rocha. UP-DOWN cortical dynamics reflect state transitions in a bistable network. *eLife*, 6:e22425, 2017.
- [105] Lauren M. Jones, Alfredo Fontanini, Brian F. Sadacca, Paul Miller, and Donald B. Katz. Natural stimuli evoke dynamic sequences of states in sensory cortical ensembles. *Proceedings of the National Academy of Sciences*, 104(47):18772–18777, 2007.

- [106] B. D. Josephson. Coupled Superconductors. *Reviews of Modern Physics*, 36(1):216–220, 1964.
- [107] Michel Jouvet. What does a cat dream about? *Trends in Neurosciences*, 2:280–282, 1979.
- [108] Vitaliy Kaminker and Renate Wackerbauer. Alternating activity patterns and a chimera-like state in a network of globally coupled excitable Morris-Lecar neurons. *Chaos: An Interdisciplinary Journal of Nonlinear Science*, 29(5):053121, 2019.
- [109] Kunihiko Kaneko and Ichiro Tsuda. Chaotic itinerancy. *Chaos*, 13(3):926, 2003.
- [110] Rajat Karnatak, Gerrit Ansmann, Ulrike Feudel, and Klaus Lehnertz. Route to extreme events in excitable systems. *Physical Review E*, 90(2):022917, 2014.
- [111] Kelso and J. A. Scott. Multistability and metastability: Understanding dynamic coordination in the brain. *Philosophical Transactions of the Royal Society B: Biological Sciences*, 367(1591):906–918, 2012.
- [112] J. A. S. Kelso and G. C. DeGuzman. An Intermittency Mechanism for Coherent and Flexible Brain and Behavioral Function. In *Tutorials in Motor Neuroscience*, pages 305–310. Springer Netherlands, 1991.
- [113] Keegan Keplinger and Renate Wackerbauer. Transient spatiotemporal chaos in the Morris-Lecar neuronal ring network. *Chaos: An Interdisciplinary Journal of Nonlinear Science*, 24(1):013126, 2014.
- [114] Mikail Khona and Ila R. Fiete. Attractor and integrator networks in the brain. *Nature Reviews Neuroscience*, 23(12):744–766, 2022.
- [115] Daniel Koch, Akhilesh Nandan, Gayathri Ramesan, and Aneta Koseska. Beyond fixed points: transient quasi-stable dynamics emerging from ghost channels and ghost cycles. *arXiv*, 2023.
- [116] Suso Kraut and Ulrike Feudel. Multistability, noise, and attractor hopping: The crucial role of chaotic saddles. *Physical Review E*, 66(1):015207, 2002.
- [117] Suso Kraut and Ulrike Feudel. Enhancement of noise-induced escape through the existence of a chaotic saddle. *Physical Review E*, 67(1):4, 2003.
- [118] Suso Kraut, Ulrike Feudel, and Celso Grebogi. Preference of attractors in noisy multistable systems. *Physical Review E*, 59(5):5253–5260, 1999.
- [119] Levin Kuhlmann, Klaus Lehnertz, Mark P. Richardson, Björn Schelter, and Hitzen P. Zaveri. Seizure prediction — ready for a new era. *Nature Reviews Neurology*, 14(10):618–630, 2018.
- [120] Yoshiki Kuramoto. Self-entrainment of a population of coupled non-linear oscillators. *International Symposium on Mathematical Problems in Theoretical Physics. Lecture Notes in Physics*, 39:420–422, 1975.

- [121] Yoshiki Kuramoto. *Chemical Oscillations, Waves, and Turbulence*, volume 19 of *Springer Series in Synergetics*. Springer Berlin Heidelberg, Berlin, Heidelberg, 1984.
- [122] Jacopo Lafranceschina and Renate Wackerbauer. Impact of weak excitatory synapses on chaotic transients in a diffusively coupled Morris-Lecar neuronal network. *Chaos: An Interdisciplinary Journal of Nonlinear Science*, 25(1):013119, 2015.
- [123] Ying-Cheng Lai and Tamás Tél. *Transient Chaos: Complex Dynamics on Finite-TIme Scales*. Applied Mathematical Sciences. Springer New York, NY, 2009.
- [124] Rodrigo Laje and Dean V Buonomano. Robust timing and motor patterns by taming chaos in recurrent neural networks. *Nature Neuroscience*, 16(7):925–933, 2013.
- [125] Liam Lang, Giancarlo La Camera, and Alfredo Fontanini. Temporal progression along discrete coding states during decision-making in the mouse gustatory cortex. *PLOS Computational Biology*, 19(2):e1010865, 2023.
- [126] Won Hee Lee and Sophia Frangou. Linking functional connectivity and dynamic properties of resting-state networks. *Scientific Reports*, 7(1):16610, 2017.
- [127] D. Lehmann, H. Ozaki, and I. Pal. EEG alpha map series: brain micro-states by space-oriented adaptive segmentation. *Electroencephalography and Clinical Neurophysiology*, 67(3):271–288, 1987.
- [128] Cheng-yu T. Li, Mu-ming Poo, and Yang Dan. Burst Spiking of a Single Cortical Neuron Modifies Global Brain State. *Science*, 324(5927):643–646, 2009.
- [129] Luisa H B Liboni, Roberto C Budzinski, Alexandra N Busch, Sindy Löwe, Thomas A Keller, Max Welling, and Lyle E Muller. Image segmentation with traveling waves in an exactly solvable recurrent neural network. *arXiv*, 2023.
- [130] Lorenz and N. Edward. Deterministic Nonperiodic Flow. *Journal of the Atmospheric Sciences*, 20(2):130–141, 1963.
- [131] Artur Luczak, Peter Barthó, Stephan L. Marguet, György Buzsáki, and Kenneth D. Harris. Sequential structure of neocortical spontaneous activity in vivo. *Proceedings of the National Academy of Sciences*, 104(1):347–352, 2007.
- [132] P. Manneville and Y. Pomeau. Intermittency and the Lorenz model. *Physics Letters A*, 75(1-2):1–2, 1979.
- [133] Eve Marder and Dirk Bucher. Central pattern generators and the control of rhythmic movements. *Current Biology*, 11(23):R986–R996, 2001.
- [134] Milos Marek and Ivan Stuchl. Synchronization in two interacting oscillatory systems. *Biophysical Chemistry*, 3(3):241–248, 1975.
- [135] George A. Mashour, Pieter Roelfsema, Jean-Pierre Changeux, and Stanislas Dehaene. Conscious Processing and the Global Neuronal Workspace Hypothesis. *Neuron*, 105(5):776–798, 2020.

- [136] Ofer Mazor and Gilles Laurent. Transient Dynamics versus Fixed Points in Odor Representations by Locust Antennal Lobe Projection Neurons. *Neuron*, 48(4):661–673, 2005.
- [137] L Mazzucato, G La Camera, and A Fontanini. Expectation-induced modulation of metastable activity underlies faster coding of sensory stimuli. *Nature Neuroscience*, 22(5):787–796, 2019.
- [138] Luca Mazzucato, Alfredo Fontanini, and Giancarlo La Camera. Dynamics of multi-stable states during ongoing and evoked cortical activity. *Journal of Neuroscience*, 35(21):8214–8231, 2015.
- [139] Everton S. Medeiros, Iberê L. Caldas, Murilo S. Baptista, and Ulrike Feudel. Trapping Phenomenon Attenuates the Consequences of Tipping Points for Limit Cycles. *Scientific Reports*, 7(1):42351, 2017.
- [140] Everton S. Medeiros, Rene O. Medrano-T, Iberê L. Caldas, and Ulrike Feudel. Boundaries of synchronization in oscillator networks. *Physical Review E*, 98(3):030201, 2018.
- [141] Everton S. Medeiros, Rene O. Medrano-T, Iberê L. Caldas, Tamás Tél, and Ulrike Feudel. State-dependent vulnerability of synchronization. *Physical Review E*, 100(5):052201, 2019. Publisher: American Physical Society.
- [142] Georgi S. Medvedev. Small-world networks of Kuramoto oscillators. *Physica D: Non-linear Phenomena*, 266:13–22, 2014.
- [143] Hildegard Meyer-Ortmanns. Heteroclinic networks for brain dynamics. *Frontiers in Network Physiology*, 3:1276401, 2023.
- [144] Christoph M. Michel and Thomas Koenig. EEG microstates as a tool for studying the temporal dynamics of whole-brain neuronal networks: A review. *NeuroImage*, 180(Pt B):577–593, 2017.
- [145] Adilson E. Motter, Seth A. Myers, Marian Anghel, and Takashi Nishikawa. Spontaneous synchrony in power-grid networks. *Nature Physics*, 9(3):191–197, 2013.
- [146] Lyle Muller, Ján Mináč, and Tung T. Nguyen. Algebraic approach to the Kuramoto model. *Physical Review E*, 104(2):L022201, 2021.
- [147] Lyle Muller, Giovanni Piantoni, Dominik Koller, Sydney S Cash, Eric Halgren, and Terrence J Sejnowski. Rotating waves during human sleep spindles organize global patterns of activity that repeat precisely through the night. *eLife*, 5:e17267, 2016.
- [148] Shruti Naik, Arpan Banerjee, Raju S. Bapi, Gustavo Deco, and Dipanjan Roy. Metastability in Senescence. *Trends in Cognitive Sciences*, 21(7):509–521, 2017. Publisher: Elsevier Current Trends.
- [149] Akhilesh Nandan, Abhishek Das, Robert Lott, and Aneta Koseska. Cells use molecular working memory to navigate in changing chemoattractant fields. *eLife*, 11:e76825, 2022.

- [150] Akhilesh Nandan and Aneta Koseska. Non-asymptotic transients away from steady states determine cellular responsiveness to dynamic spatial-temporal signals. *PLOS Computational Biology*, 19(8):e1011388, 2023.
- [151] John C. Neu. Chemical Waves and the Diffusive Coupling of Limit Cycle Oscillators. *SIAM Journal on Applied Mathematics*, 36(3):509–515, 1979.
- [152] M E Newman and D J Watts. Scaling and percolation in the small-world network model. *Physical Review E*, 60(6 Pt B):7332–7342, 1999.
- [153] Micha Nixon, Moti Friedman, Eitan Ronen, Asher A. Friesem, Nir Davidson, and Ido Kanter. Synchronized Cluster Formation in Coupled Laser Networks. *Physical Review Letters*, 106(22):223901, 2011.
- [154] Thomas Nowotny and Mikhail I Rabinovich. Dynamical Origin of Independent Spiking and Bursting Activity in Neural Microcircuits. *Physical Review Letters*, 98(12):128106, 2007.
- [155] Enzo Olivieri and Maria Eulália Vares. *Large Deviations and Metastability*. Encyclopedia of Mathematics and its Applications. Cambridge University Press, Cambridge, 2005.
- [156] Edward Ott. *Chaos in Dynamical Systems*. Cambridge University Press, Cambridge, U.K, 2nd edition edition, 2022.
- [157] Edward Ott and John C. Sommerer. Blowout bifurcations: the occurrence of riddled basins and on-off intermittency. *Physics Letters A*, 188(1):39–47, 1994.
- [158] Franziska Peter and Arkady Pikovsky. Transition to collective oscillations in finite Kuramoto ensembles. *Physical Review E*, 97(3):032310, 2018.
- [159] Arkady Pikovsky, Michael Rosenblum, and Jürgen Kurths. *Synchronization: A Universal Concept in Nonlinear Science*, volume 70. Cambridge University Press, 2001.
- [160] Alexander N. Pisarchik and Ulrike Feudel. Control of multistability. *Physics Reports*, 540(4):167–218, 2014.
- [161] N Platt, E A Spiegel, and C Tresser. On-off intermittency: A mechanism for bursting. *Physical Review Letters*, 70(3):279–282, 1993.
- [162] Yves Pomeau and Paul Manneville. Intermittent transition to turbulence in dissipative dynamical systems. *Communications in Mathematical Physics*, 74(2):189–197, 1980.
- [163] Adrián Ponce-Alvarez, Gustavo Deco, Patric Hagmann, Gian Luca Romani, Dante Mantini, and Maurizio Corbetta. Resting-State Temporal Synchronization Networks Emerge from Connectivity Topology and Heterogeneity. *PLOS Computational Biology*, 11(2):e1004100, 2015.

- [164] D Popa, A T Popescu, and D Pare. Contrasting Activity Profile of Two Distributed Cortical Networks as a Function of Attentional Demands. *Journal of Neuroscience*, 29(4):1191–1201, 2009.
- [165] James F. A. Poulet and Carl C. H. Petersen. Internal brain state regulates membrane potential synchrony in barrel cortex of behaving mice. *Nature*, 454(7206):881–885, 2008.
- [166] M. Rabinovich, A. Volkovskii, P. Lecanda, R. Huerta, H. D. I. Abarbanel, and G. Laurent. Dynamical Encoding by Networks of Competing Neuron Groups: Winnerless Competition. *Physical Review Letters*, 87(6):068102, 2001.
- [167] Mikhail I Rabinovich, Valentin S Afraimovich, Christian Bick, and Pablo Varona. Information flow dynamics in the brain. *Physics of life reviews*, 9(1):51–73, 2012.
- [168] Mikhail I. Rabinovich, Ramón Huerta, Pablo Varona, and Valentin S. Afraimovich. Transient cognitive dynamics, metastability, and decision making. *PLoS Computational Biology*, 4(5):1000072, 2008.
- [169] Mikhail I. Rabinovich, Pablo Varona, Irma Tristan, and Valentin S. Afraimovich. Chunking dynamics: heteroclinics in mind. *Frontiers in Computational Neuroscience*, 8:22, 2014.
- [170] Misha Rabinovich, Ramon Huerta, and Gilles Laurent. Transient Dynamics for Neural Processing. *Science*, 321(5885):48–50, 2008.
- [171] Christopher Rackauckas and Qing Nie. DifferentialEquations.jl – A Performant and Feature-Rich Ecosystem for Solving Differential Equations in Julia. *Journal of Open Research Software*, 5(1):15, 2016.
- [172] Stefano Recanatesi, Ulises Pereira-Obilinovic, Masayoshi Murakami, Zachary Mainen, and Luca Mazzucato. Metastable attractors explain the variable timing of stable behavioral action sequences. *Neuron*, 2021.
- [173] Thorsten Rings, Mahmood Mazarei, Amin Akhshi, Christian Geier, M. Reza Rahimi Tabar, and Klaus Lehnertz. Traceability and dynamical resistance of precursor of extreme events. *Scientific Reports*, 9(1):1744, 2019.
- [174] James A Roberts, Leonardo L Gollo, Romesh G Abeysuriya, Gloria Roberts, Philip B Mitchell, Mark W Woolrich, and Michael Breakspear. Metastable brain waves. *Nature Communications*, 10(1):1056, 2019.
- [175] Francisco A. Rodrigues, Thomas K.D.M. Peron, Peng Ji, and Jürgen Kurths. The Kuramoto model in complex networks. *Physics Reports*, 610:1–98, 2016.
- [176] Jeffrey L. Rogers and Luc T. Wille. Phase transitions in nonlinear oscillator chains. *Physical Review E*, 54(3):R2193–R2196, 1996.

- [177] M G Rosenblum, A S Pikovsky, and J Kurths. Phase synchronization of chaotic oscillators. *Physical Review Letters*, 76(11):1804–1807, 1996.
- [178] K. L. Rossi. Repository for metastability. *Github repository*, 2023. <https://github.com/ComplexNetworks-jl/MetastableDynamics>.
- [179] Kalel Rossi. Repository for dynamical malleability code. *Github Repository*, 2022.
- [180] Horacio G. Rotstein. Mixed-Mode Oscillations in Single Neurons. In Jaeger Dieter and Jung Ranu, editors, *Encyclopedia of Computational Neuroscience*, Encyclopedia of Computational Neuroscience, pages 1–9. Springer New York, NY, 2014.
- [181] Mikail Rubinov, Rolf J F Ypma, Charles Watson, and Edward T Bullmore. Wiring cost and topological participation of the mouse brain connectome. *Proceedings of the National Academy of Sciences of the United States of America*, 112(32):10032–10037, 2015.
- [182] Arindam Saha and Ulrike Feudel. Extreme events in FitzHugh-Nagumo oscillators coupled with two time delays. *Physical Review E*, 95(6):062219, 2017.
- [183] Arindam Saha and Ulrike Feudel. Characteristics of in-out intermittency in delay-coupled FitzHugh–Nagumo oscillators. *The European Physical Journal Special Topics*, 227(10-11):1205–1219, 2018.
- [184] Akira Sakurai, Arianna N. Tamvacakis, and Paul S. Katz. Recruitment of Polysynaptic Connections Underlies Functional Recovery of a Neural Circuit after Lesion. *eNeuro*, 3(4), 2016.
- [185] T Sasaki, N Matsuki, and Y Ikegaya. Metastability of Active CA3 Networks. *Journal of Neuroscience*, 27(3):517–528, 2007.
- [186] E Seidemann, I Meilijson, M Abeles, H Bergman, and E Vaadia. Simultaneously recorded single units in the frontal cortex go through sequences of discrete and stable states in monkeys performing a delayed localization task. *The Journal of Neuroscience*, 16(2):752–768, 1996.
- [187] W Singer. Neuronal synchrony: a versatile code for the definition of relations? *Neuron*, 24(1):49–65,111, 1999.
- [188] Per Sebastian Skardal and Alex Arenas. Higher order interactions in complex networks of phase oscillators promote abrupt synchronization switching. *Communications Physics*, 3(1):218, 2020.
- [189] Per Sebastian Skardal, Dane Taylor, and Jie Sun. Optimal Synchronization of Complex Networks. *Physical Review Letters*, 113(14):144101, 2014.
- [190] Didier Sornette. *Critical Phenomena in Natural Sciences, Chaos, Fractals, Selforganization and Disorder: Concepts and Tools*. Springer Series in Synergetics. 2006.

- [191] Mircea Steriade, David A. McCormick, and Terrence J. Sejnowski. Thalamocortical Oscillations in the Sleeping and Aroused Brain. *Science*, 262(5134):679–685, 1993.
- [192] Strogatz. *Nonlinear Dynamics and Chaos*. Studies in nonlinearity. Westview, 2002.
- [193] Steven H. Strogatz and Renato E. Mirollo. Phase-locking and critical phenomena in lattices of coupled nonlinear oscillators with random intrinsic frequencies. *Physica D: Nonlinear Phenomena*, 31(2):143–168, 1988.
- [194] David Sussillo and Omri Barak. Opening the Black Box: Low-Dimensional Dynamics in High-Dimensional Recurrent Neural Networks. *Neural Computation*, 25(3):626–649, 2013.
- [195] H A Swadlow and A G Gusev. The impact of 'bursting' thalamic impulses at a neocortical synapse. *Nature Neuroscience*, 4(4):402–408, 2001.
- [196] M. Reza Rahini Tabar. *Analysis and Data-Based Reconstruction of Complex Nonlinear Dynamical Systems, Using the Methods of Stochastic Processes*. Understanding Complex Systems. Springer Cham, 2019.
- [197] Dane Taylor, Per Sebastian Skardal, and Jie Sun. Synchronization of Heterogeneous Oscillators Under Network Modifications: Perturbation and Optimization of the Synchrony Alignment Function. *SIAM Journal on Applied Mathematics*, 76(5):1984–2008, 2016.
- [198] Richard Taylor. There is no non-zero stable fixed point for dense networks in the homogeneous Kuramoto model. *Journal of Physics A: Mathematical and Theoretical*, 45(5):055102, 2012.
- [199] Qawi K. Telesford, Karen E. Joyce, Satoru Hayasaka, Jonathan H. Burdette, and Paul J. Laurienti. The Ubiquity of Small-World Networks. *Brain Connectivity*, 1(5):367–375, 2011.
- [200] Paulo F. C. Tilles, Fernando F. Ferreira, and Hilda A. Cerdeira. Multistable behavior above synchronization in a locally coupled Kuramoto model. *Physical Review E*, 83(6):066206, 2011.
- [201] Emmanuelle Tognoli and J. A. Scott Kelso. Enlarging the scope: grasping brain complexity. *Frontiers in Systems Neuroscience*, 8:122, 2014.
- [202] Emmanuelle Tognoli and J. A. Scott Kelso. The Metastable Brain. *Neuron*, 81(1):35–48, 2014.
- [203] G Tononi, O Sporns, and G M Edelman. A measure for brain complexity: relating functional segregation and integration in the nervous system. *Proceedings of the National Academy of Sciences*, 91(11):5033–5037, 1994.
- [204] Giulio Tononi and Gerald M. Edelman. Consciousness and Complexity. *Science*, 282(5395):1846–1851, 1998.

- [205] Alex Townsend, Michael Stillman, and Steven H. Strogatz. Dense networks that do not synchronize and sparse ones that do. *Chaos: An Interdisciplinary Journal of Nonlinear Science*, 30(8):083142, 2020.
- [206] Rory G. Townsend, Selina S. Solomon, Spencer C. Chen, Alexander N.J. Pietersen, Paul R. Martin, Samuel G. Solomon, and Pulin Gong. Emergence of Complex Wave Patterns in Primate Cerebral Cortex. *The Journal of Neuroscience*, 35(11):4657–4662, 2015.
- [207] Ichiro Tsuda. Hypotheses on the functional roles of chaotic transitory dynamics. *Chaos: An Interdisciplinary Journal of Nonlinear Science*, 19(1):015113, 2009.
- [208] Ichiro Tsuda. Chaotic itinerancy and its roles in cognitive neurodynamics. *Current Opinion in Neurobiology*, 31:67–71, 2015.
- [209] F Varela, J P Lachaux, E Rodriguez, and J Martinerie. The brainweb: phase synchronization and large-scale integration. *Nature Reviews Neuroscience*, 2(4):229–239, 2001.
- [210] J. L. Perez Velazquez, Houman Khosravani, Andres Lozano, Berj. L. Bardakjian, Peter L. Carlen, and Richard Wennberg. Type III intermittency in human partial epilepsy. *European Journal of Neuroscience*, 11(7):2571–2576, 1999.
- [211] Dimitri Van De Ville, Juliane Britz, and Christoph M. Michel. EEG microstate sequences in healthy humans at rest reveal scale-free dynamics. *Proceedings of the National Academy of Sciences*, 107(42):18179–18184, 2010.
- [212] Pablo Villegas, Paolo Moretti, and Miguel A. Muñoz. Frustrated hierarchical synchronization and emergent complexity in the human connectome network. *Scientific Reports*, 4(1):5990, 2014.
- [213] Henning U. Voss, Jens Timmer, and Jürgen Kurths. Nonlinear dynamical system identification from uncertain and indirect measurements. *International Journal of Bifurcation and Chaos*, 14(06):1905–1933, 2004.
- [214] František Váša, Murray Shanahan, Peter J. Hellyer, Gregory Scott, Joana Cabral, and Robert Leech. Effects of lesions on synchrony and metastability in cortical networks. *NeuroImage*, 118:456–467, 2015.
- [215] Wang and Xiao-Jing. 50 years of mnemonic persistent activity: quo vadis? *Trends in Neurosciences*, 44(11):888–902, 2021.
- [216] D J Watts and S H Strogatz. Collective dynamics of ‘small-world’ networks. *Nature*, 393(6684):440–442, 1998.
- [217] Michael Wenzel, Jordan P Hamm, Darcy S Peterka, and Rafael Yuste. Acute Focal Seizures Start As Local Synchronizations of Neuronal Ensembles. *The Journal of Neuroscience*, 39(43):8562–8575, 2019.

- [218] Gerhard Werner. Metastability, criticality and phase transitions in brain and its models. *BioSystems*, 90(2):496–508, 2007.
- [219] Shai Wiseman and Eytan Domany. Lack of self-averaging in critical disordered systems. *Physical Review E*, 52(4):3469–3484, 1995.
- [220] Dirk Witthaut, Frank Hellmann, Jürgen Kurths, Stefan Kettemann, Hildegard Meyer-Ortmanns, and Marc Timme. Collective nonlinear dynamics and self-organization in decentralized power grids. *Reviews of Modern Physics*, 94(1):015005, 2022.
- [221] James A. Yorke and Ellen D. Yorke. Metastable chaos: The transition to sustained chaotic behavior in the Lorenz model. *Journal of Statistical Physics*, 21(3):263–277, 1979.
- [222] Yuanzhao Zhang and Steven H. Strogatz. Basins with Tentacles. *Physical Review Letters*, 127(19):194101, 2021.
- [223] A. Čenys, A. N. Anagnostopoulos, and G. L. Bleris. Symmetry between laminar and burst phases for on-off intermittency. *Physical Review E*, 56(3):2592–2596, 1997.